

WARSAW UNIVERSITY OF TECHNOLOGY
THE FACULTY OF POWER AND AERONAUTICAL ENGINEERING
DIVISION OF AERODYNAMICS



INTERMEDIATE PROJECT
ELABORATION OF OPTIMAL DESIGN OF BLOOD PUMP FOR MEDICAL APPLICATIONS

OMAR SALLOUM

ID 322624

Table of Contents

1.	PROJECT OBJECTIVES AND THEORETICAL INTRODUCTION OF THE PROBLEM	4
2.	GEOMETRY	5
3.	ANALYSES OF BLOOD FLOW THROUGH THE IMPELLER	8
3.1	FIRST CONFIGURATION.....	8
3.1.1	FIRST SIMULATION	8
3.1.2	SECOND SIMULATION	15
3.1.3	COMPARISON.....	20
3.2	SECOND CONFIGURATION	21
3.2.1	FIRST SIMULATION	21
3.2.2	SECOND SIMULATION	26
3.2.3	COMPARISON.....	31
3.3	THIRD CONFIGURATION	32
3.3.1	FIRST SIMULATION	32
3.3.2	SECOND SIMULATION	38
3.3.3	COMPARISON.....	44
4.	SUMMARY	45
	REFERENCES	46

1. PROJECT OBJECTIVES AND THEORETICAL INTRODUCTION OF THE PROBLEM

The main aim of the project is to elaborate on the most optimal geometry of a blood pump in terms of the shear stress, that seems to have the biggest impact on the damage of red blood cells.

Blood pumps are used to replace the beating heart during heart surgery. They propel blood and other physiologic fluids throughout the extracorporeal circuit; which includes the patient's natural circulation as well as the artificial one.

The ideal blood pump should:

- Move volumes of blood up to 5.0 L/Min
- Must be able to pump blood at low velocities of flow
- All parts in contact with blood should have smooth surface
- Must be possible to dismantle, clean and sterilize the pump with ease, and the blood handling components must be disposable
- Must have adjustable stroke volume and pulse rate

The basic mechanism of mechanical hemolysis is mentioned shear stress acting on the red blood cells, which produces tension in the membrane. If a certain momentum (the product of shear stress and exposure time) is exceeded, the hemoglobin is released into the plasma. A lethal membrane tension in the range of 0.01 N/m to 0.03 N/m depending on loading time has been reported. [1]

Shear forces are higher in areas of turbulence and, particularly in those areas with a short dimension, there is an increase in hemolysis.

Shear forces on RBCs are also increased if direct contact between the cells and the wall become more frequent. [2]

2. GEOMETRY

In this project axial blood impeller was chosen and designed in NX CAD programme. Figure 1 shows the designed impeller (first configuration).

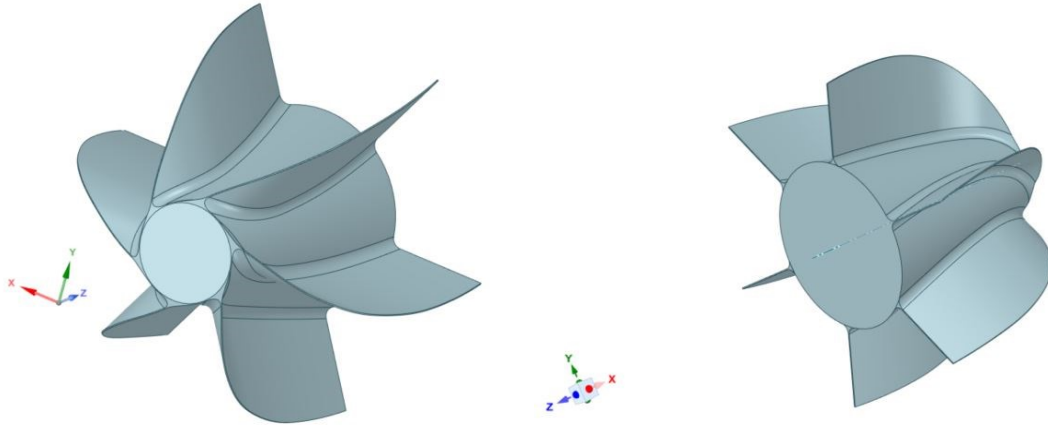


Figure 1 First configuration of the axial flow impeller.

For the purposes of flow analysis the pipe was added, in order to maintain propulsor calculations. Figure 2 shows the first configuration of the impeller inside the pipe.

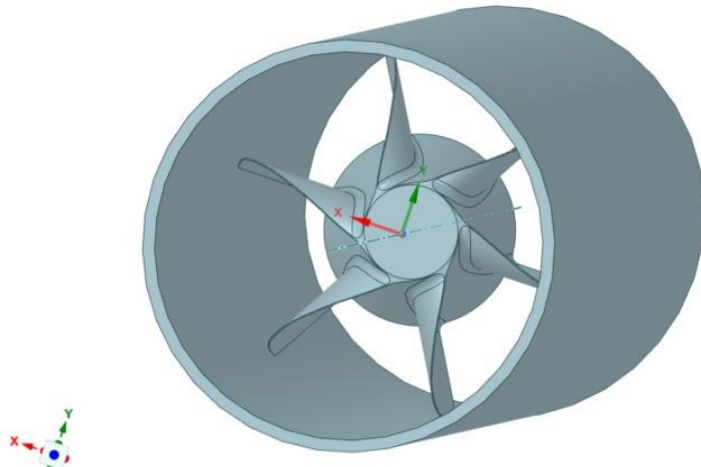


Figure 2 Impeller inside a pipe

For the elaboration of optimal design, two modifications in the geometry were made.

In the first modification, the impeller was modified by extruding a hole through the impeller. Figure 3 shows the second modification.

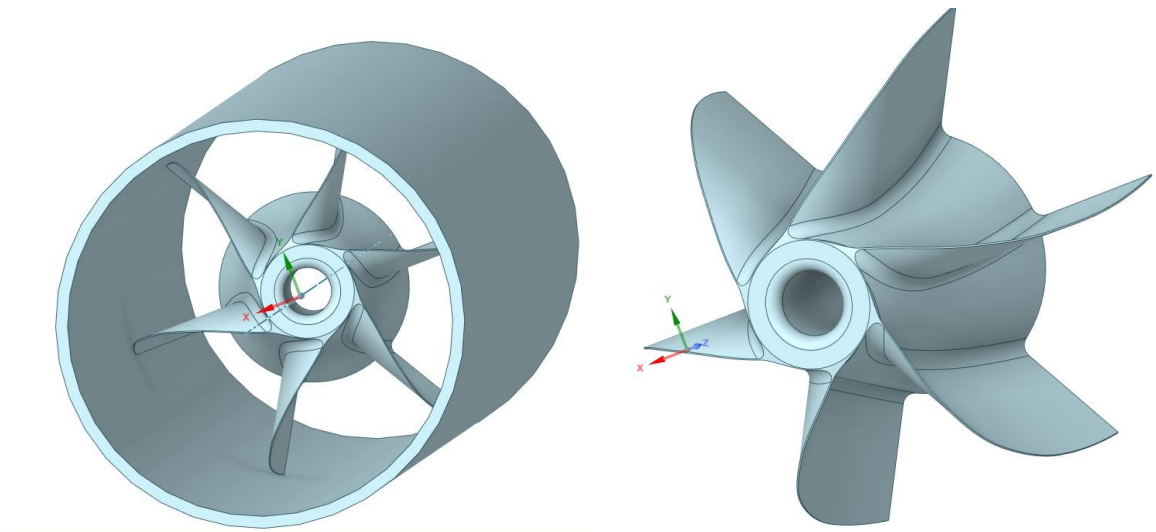


Figure 3 Second modification of the impeller

The third modification of the geometry is a concept, that applying an initial rotational flow of the blood before the impeller could potentially decrease the average value of the shear stress. Figure 4 and Figure 5 show the third configuration of the geometry.

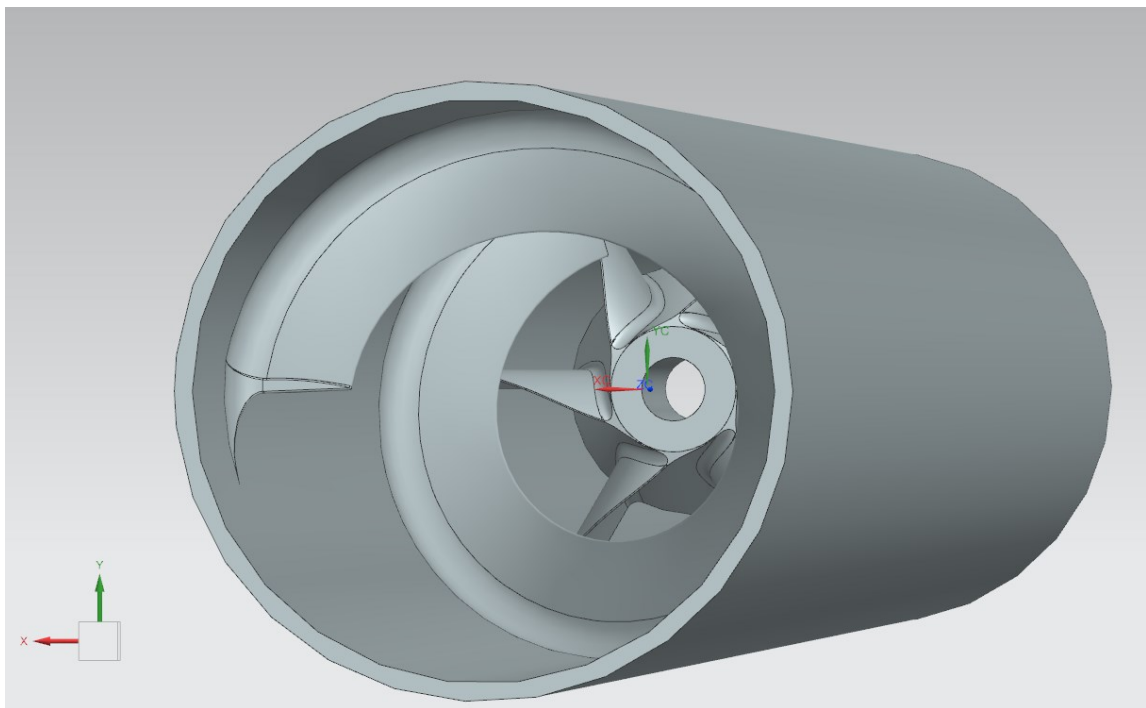


Figure 4 Third configuration of the geometry – isometric view

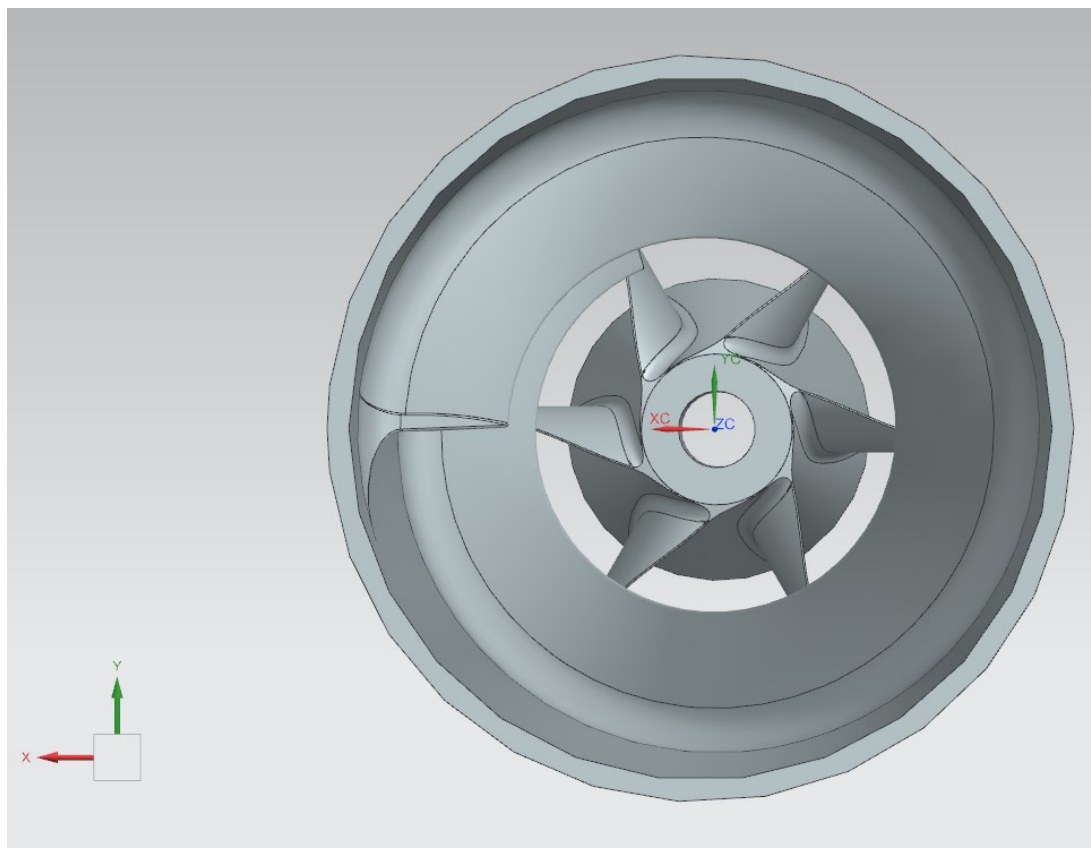


Figure 5 Third configuration of the geometry – front section

3. ANALYSES OF BLOOD FLOW THROUGH THE IMPELLER

Flow analyses and meshing were made in ANSYS FLUENT 2022 R1. For each configuration two simulations were conducted, namely for inlet velocity 0.3 m/s and 0.6 m/s. The second value of velocity were applied in order to validate the results (for example: higher velocity – higher value of the Wall Shear Stress). Meshing was made with the watertight geometry workflow.

3.1 FIRST CONFIGURATION

3.1.1 FIRST SIMULATION

First simulation was made for velocity inlet = 0.3 m/s. Value of density was taken as $\rho_{blood} = 1060 \text{ kg/m}^3$. As a viscous model the k-omega SST model was chosen. For pressure outlet – Gauge Pressure was set to 0 Pa. Impeller and pipe were set as a wall boundary. Simulation was set to Pressure-Based and Steady.

Figure 6 and Figure 7 shows the axial velocity (Z - velocity) before and after the impeller.

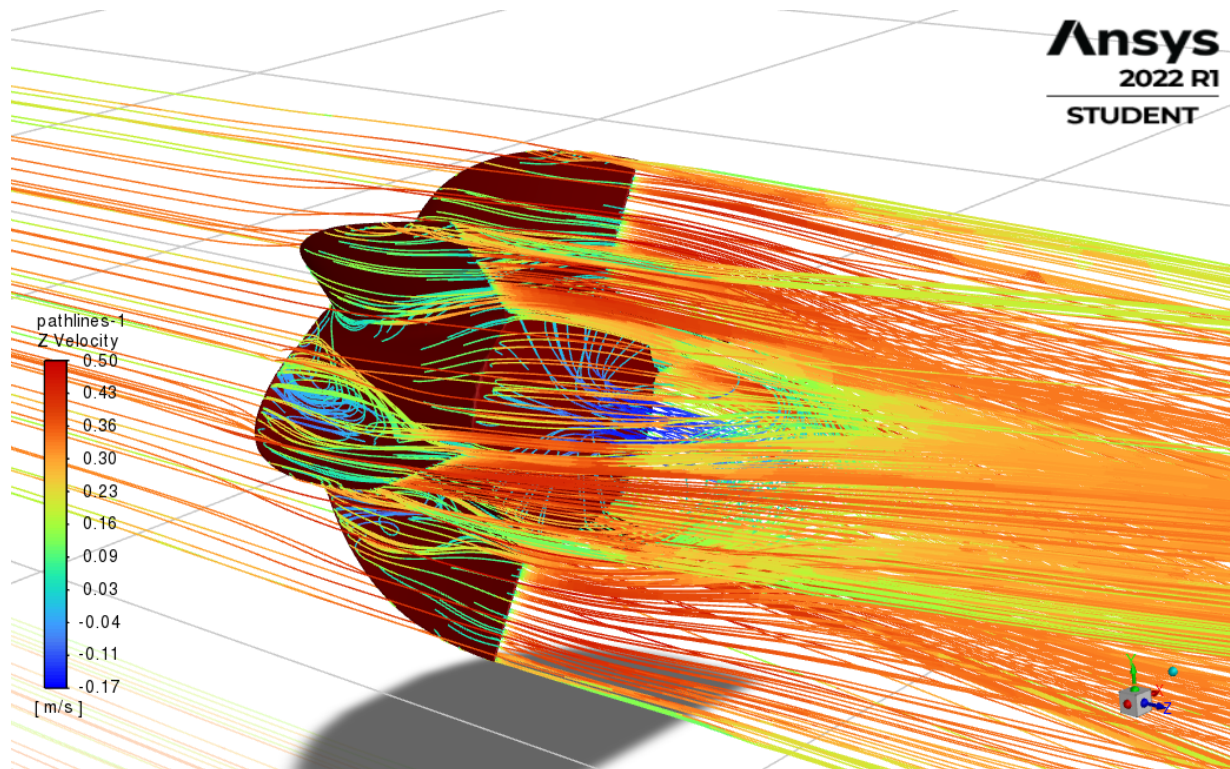


Figure 6 Axial velocity after the impeller

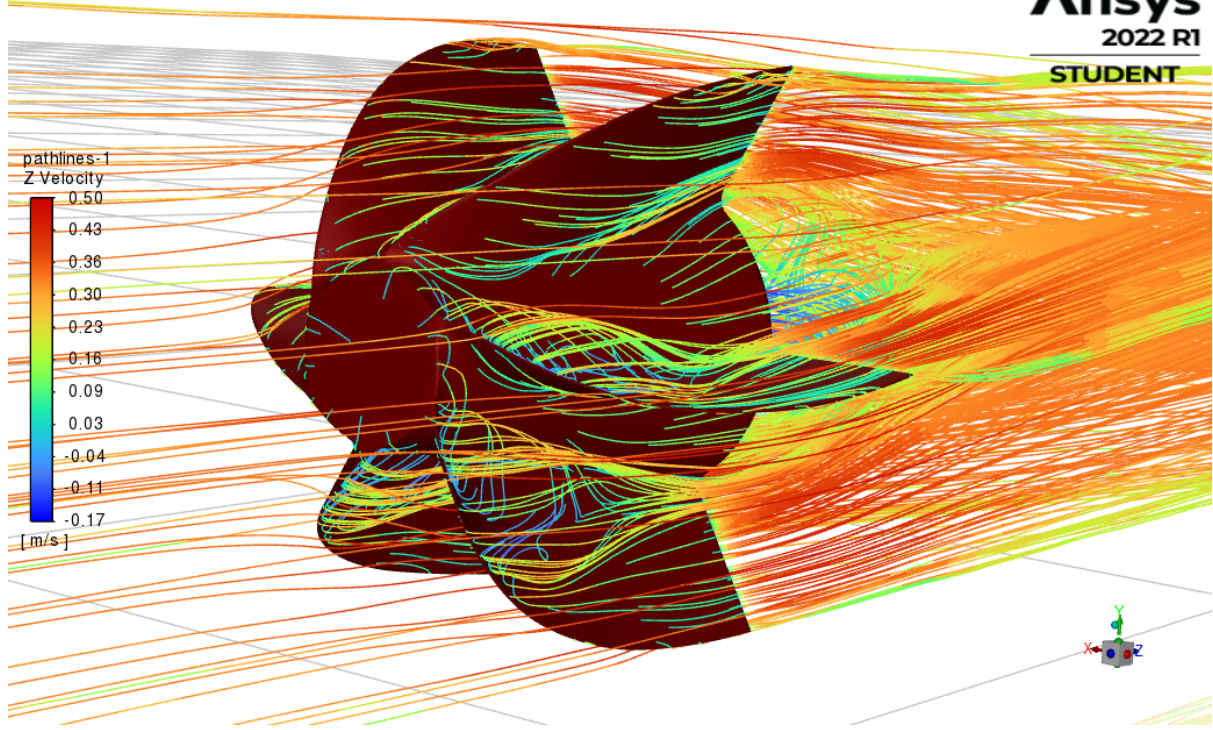


Figure 7 Axial velocity before the impeller

Pictures above show that after the pump there is a separation of flow (separation bubble), thus in terms of optimization of geometry the end of the impeller could be elongated, so that separation might be reduced.

The next observation is generation of vortices after the leading edge of the blade of the impeller due the sharp geometry of the blade's profile. Therefore, to optimize the flow through the blood pump, changes in the blade's profile shape (in particular blunting sharp geometries like for the leading edge and trailing edge) are needed.

Figure 8 shows the velocity vectors (velocity magnitude) for a flow through a pipe.

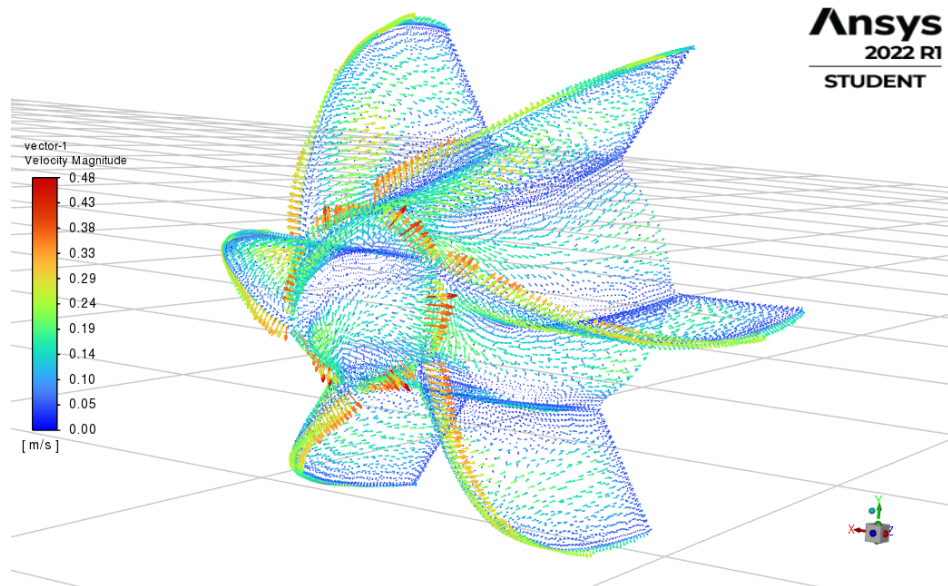


Figure 8 Velocity vectors – velocity magnitude

In the figure 8 one could observe, that the velocity of the flow is dramatically reduced on the front face of the impeller, thus creating a hole through that face could decrease that reduction, thus smaller values of Wall Shear Stresses could be obtained.

Figure 9 and figure 10 show pathlines of Y – Wall Shear Stress, and Z – Wall Shear Stress for the analysed flow.

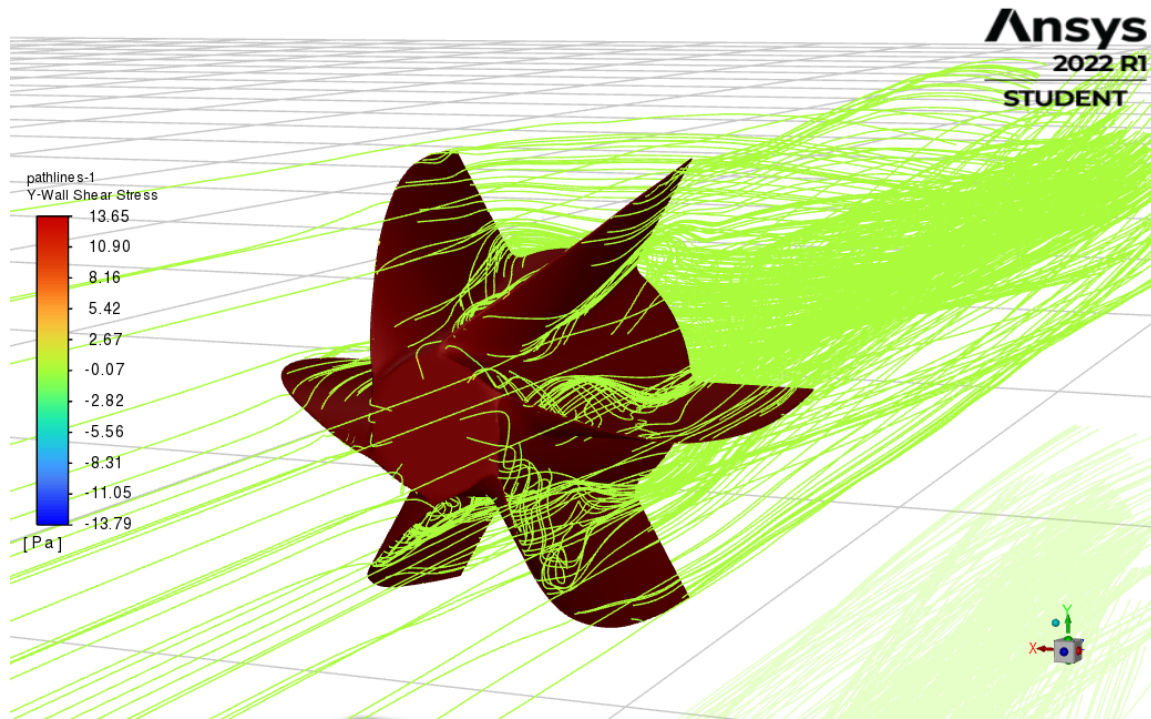


Figure 9 Pathlines of Y – Wall Shear Stress

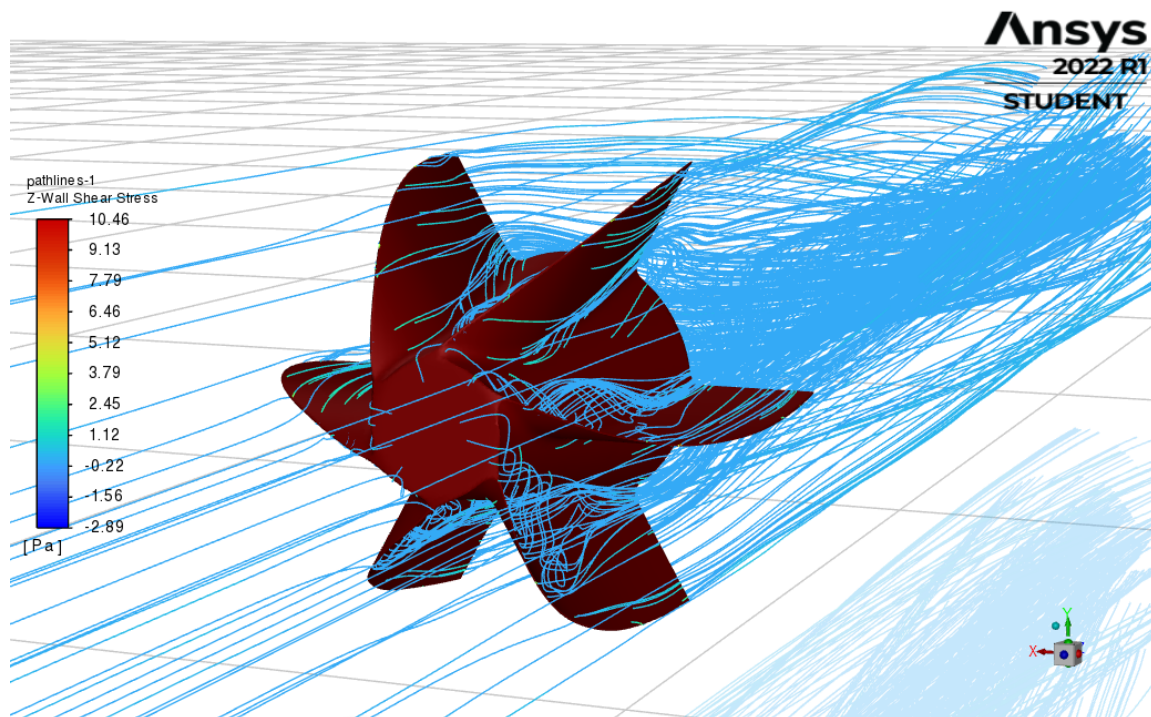


Figure 10 Pathlines of Z – Wall Shear Stress

Due to the rotation of the impeller values of Y – WWS are higher than for the axial Z-WSS.

Figure 11 shows the contours of Z-Wall Shear Stress on the surface of the impeller.

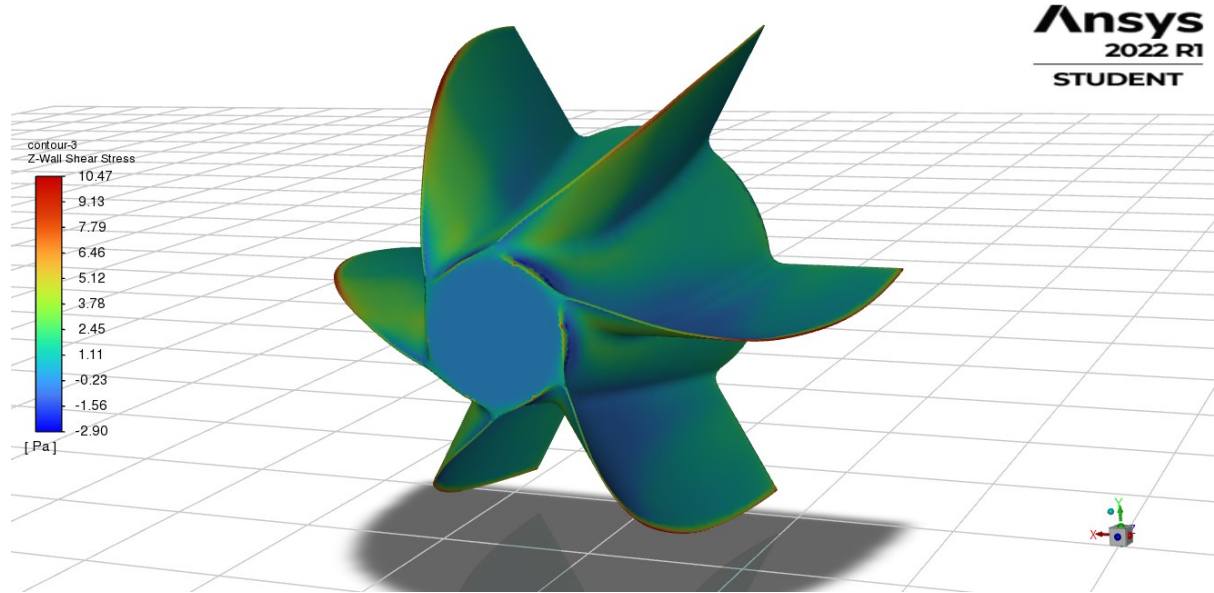


Figure 11 Contours of Z-WSS on the surface of the impeller

As it was expected, the highest value of Z-WSS are obtained on the sharp geometry, which is in this case the leading edge of the impeller's blade.

Figure 12 shows the profile of Z-WSS through the impeller as the X-Y plot.

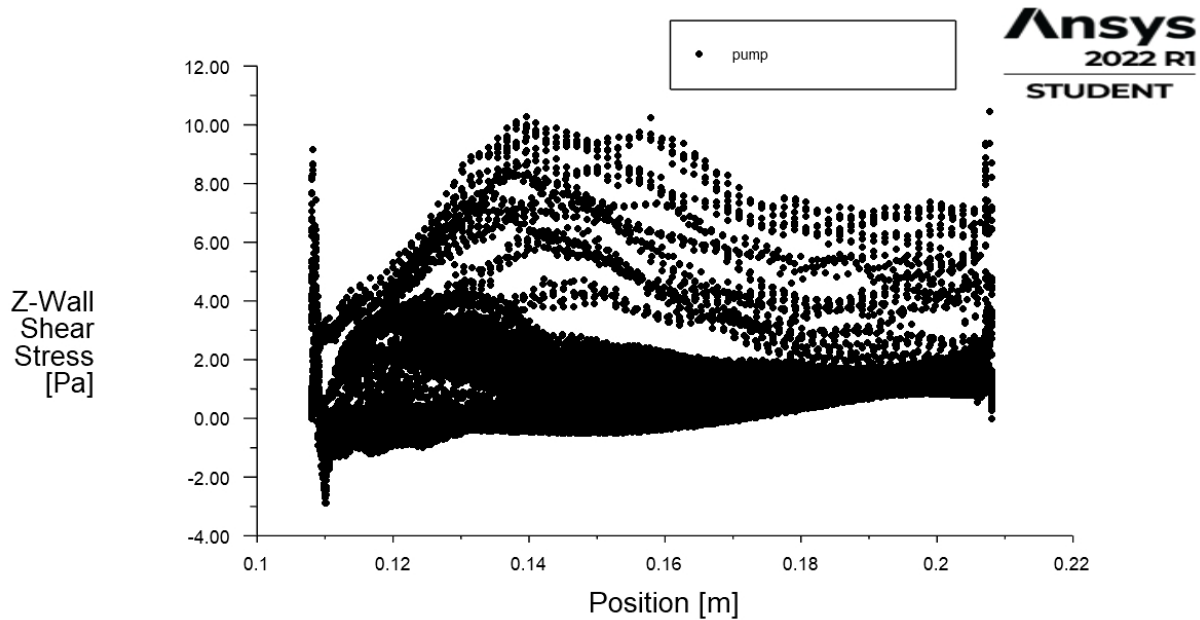


Figure 12 Characteristics of Z-WSS through the impeller

Two peaks of the Z-WSS can be observed, namely at the front face of the impeller and the back of the impeller, mostly due to the lack of the continuity of the geometry, therefore for further optimization modifications in those are desirable.

For different visual representation of the WSS, particle tracks simulation were done for YZ plane (as it is shown in figure 13).

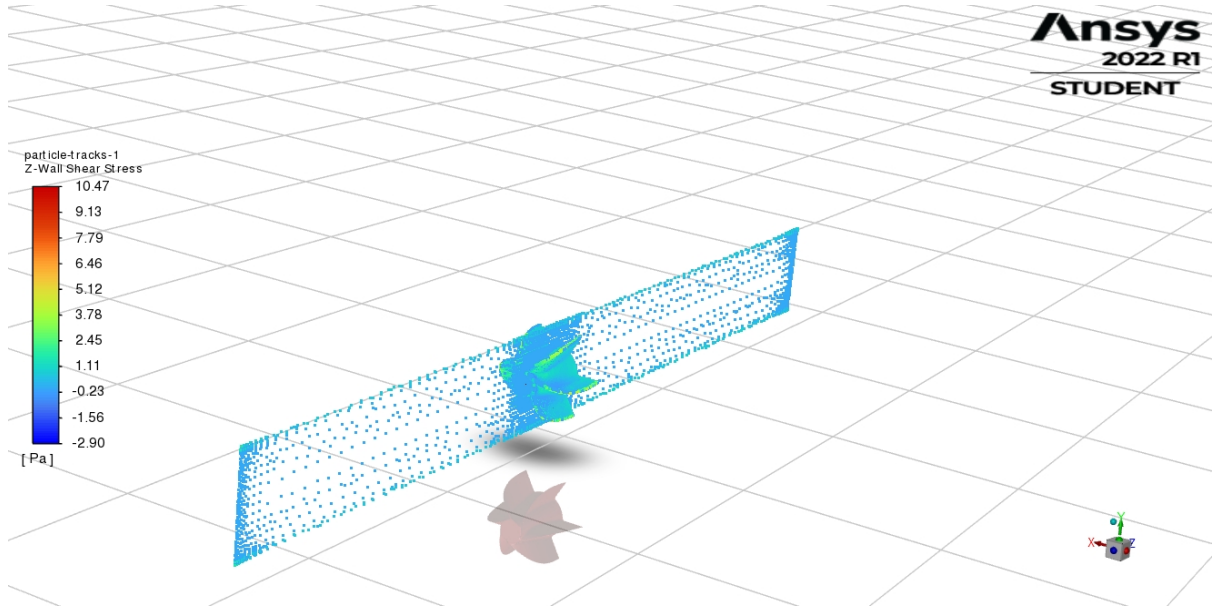


Figure 13 Particle traces in YZ plane for Z-WSS

To observe the value of Z-WSS between the blades of the impeller, this particular YZ plane was located between the blades (as it is shown in figure 14).

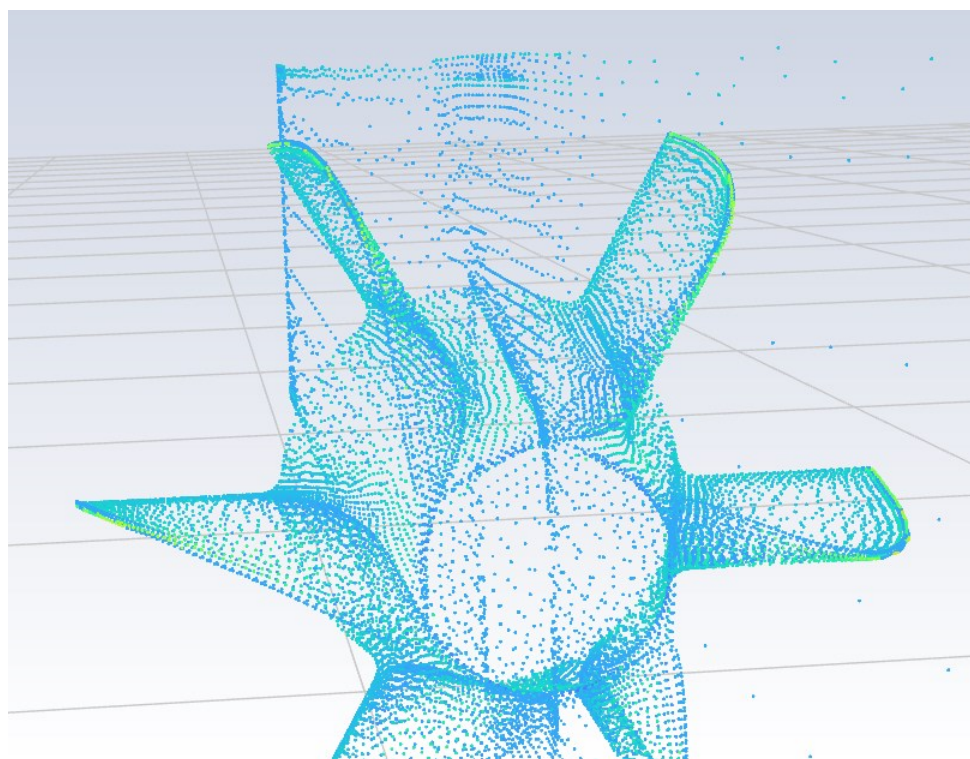


Figure 14 Location of YZ plane

For the above plane the following results of Z-WSS and Y-WSS were obtained.

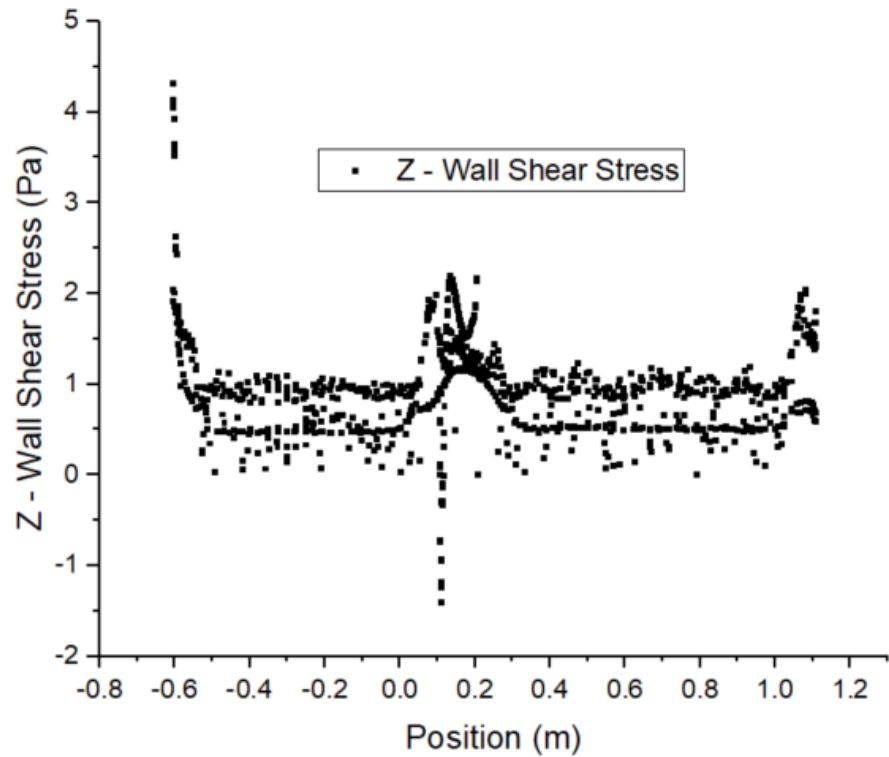


Figure 15 Z-WSS for YZ – plane (between blades)

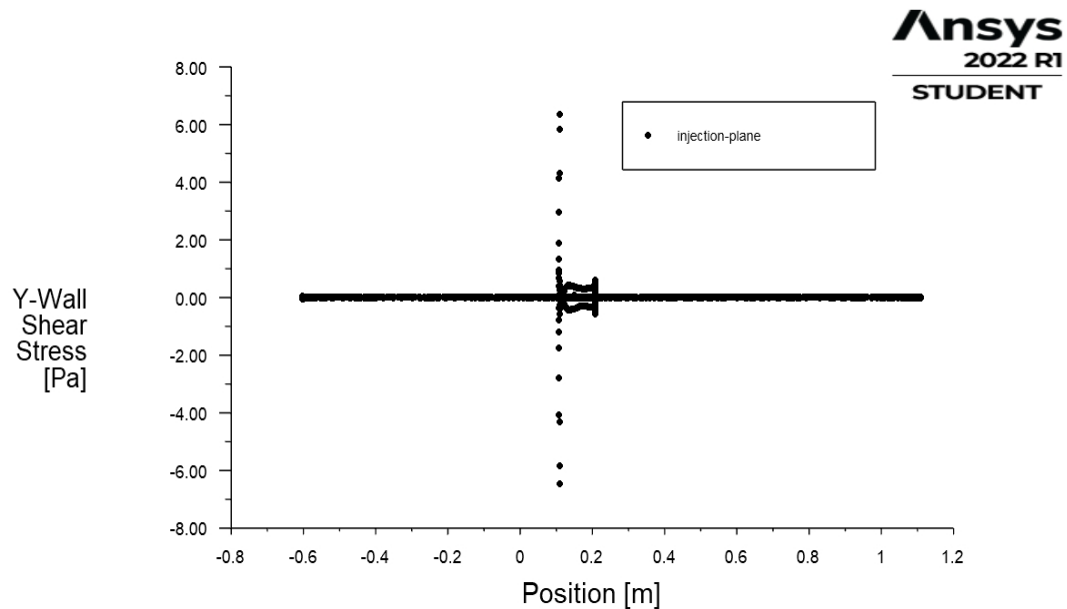


Figure 16 Y-WSS for YZ – plane (between blades)

The last part for this simulation was to calculate the Hydraulic Resistance R_H (solution from Ansys fluent):

$$R_H = \frac{\Delta p}{Q}$$

From Fluent value of hydraulic resistance is as follows (First configuration, first simulation):

$$R_H = \frac{\Delta p}{Q} = \frac{12\ 000}{2.88 * 10^{-10}} = 4.17 * 10^{13} \frac{kg}{m^4 s}$$

3.1.2 SECOND SIMULATION

Second simulation was made mainly to validate the results of the first simulation. The only change was made for the inlet velocity = 0.6 m/s (higher velocity value – higher values of WSS are expected).

Figure 17 and 18 shows the axial velocity (Z - velocity) before and after the impeller.

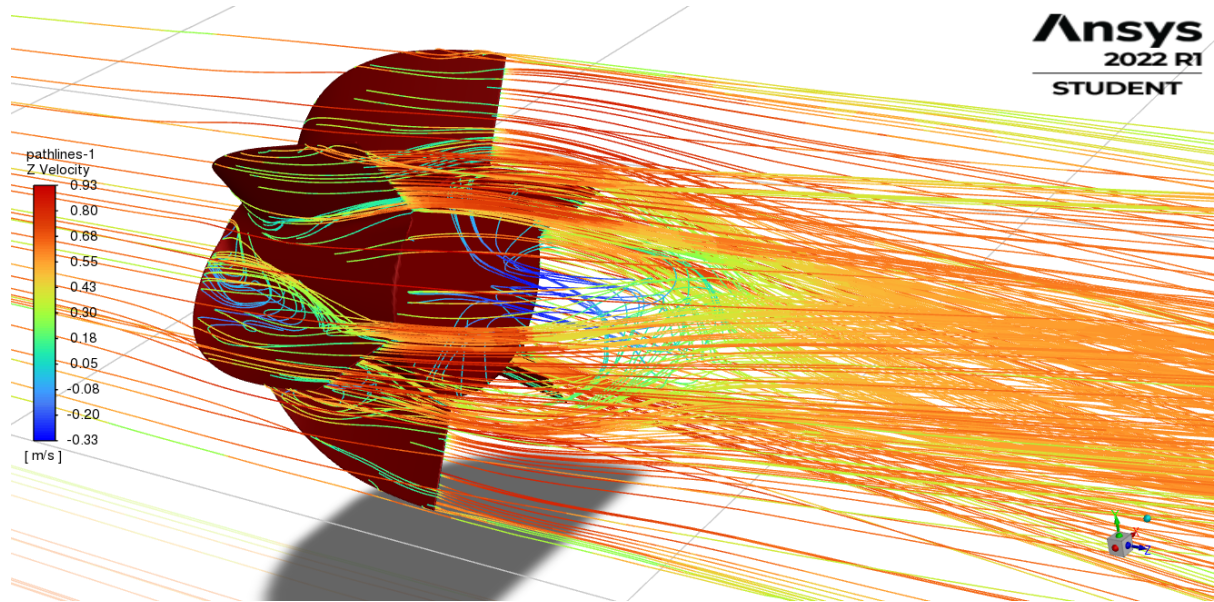


Figure 17 Axial velocity after the impeller.

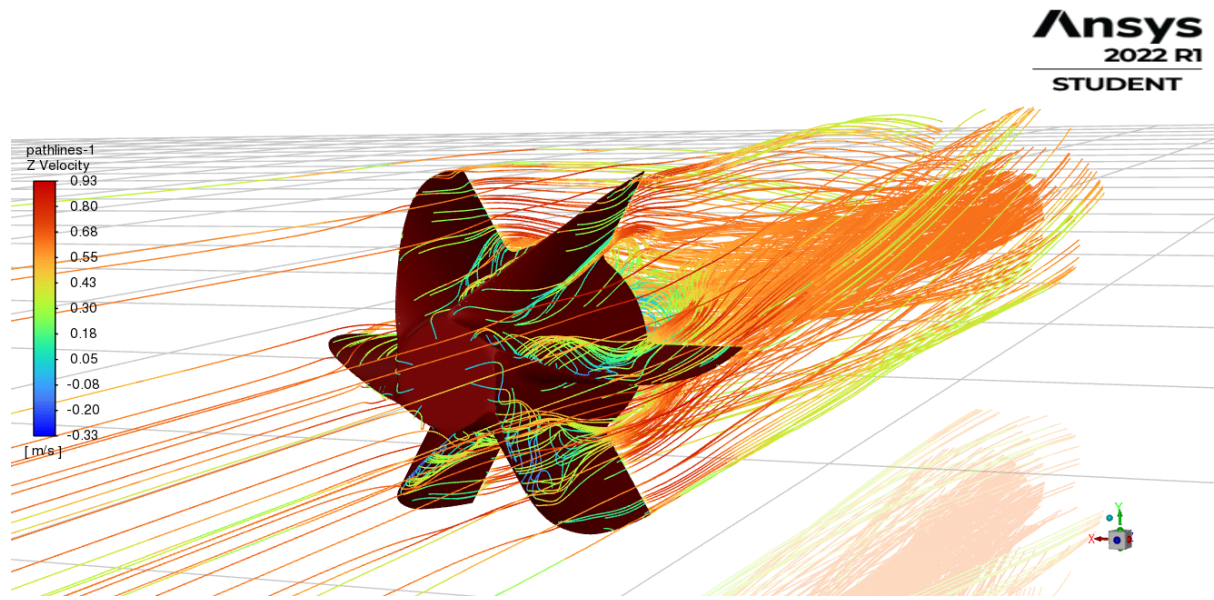


Figure 18 Axial velocity before the impeller

The phenomena are the same as in the first simulation and as expected values of velocity are higher.

Figure 19 shows the velocity vectors (velocity magnitude) for a flow through a pipe.

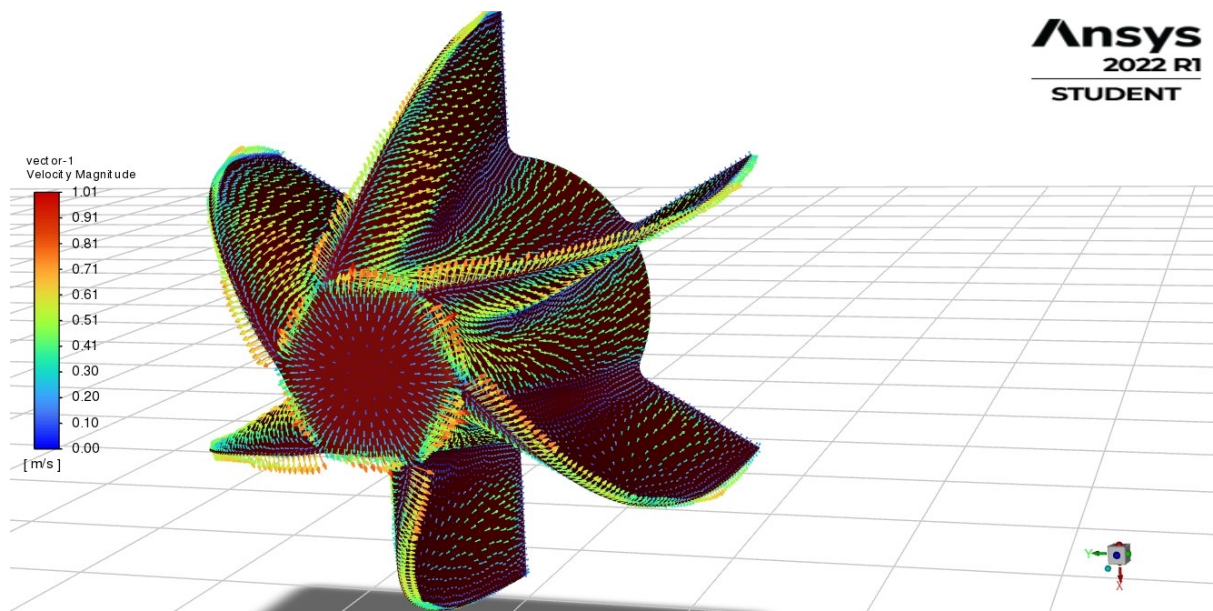


Figure 19 Velocity vectors – velocity magnitude

Figure 9 and figure 10 show pathlines of Y – Wall Shear Stress, and Z – Wall Shear Stress for the analysed flow.

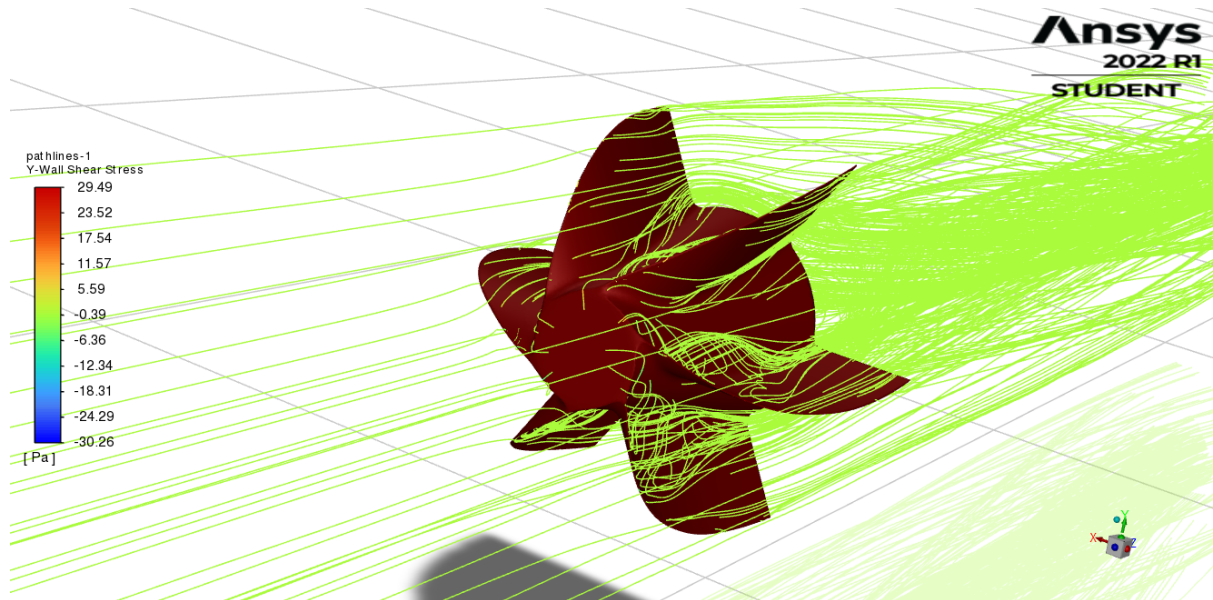


Figure 20 Pathlines of Y – Wall Shear Stress

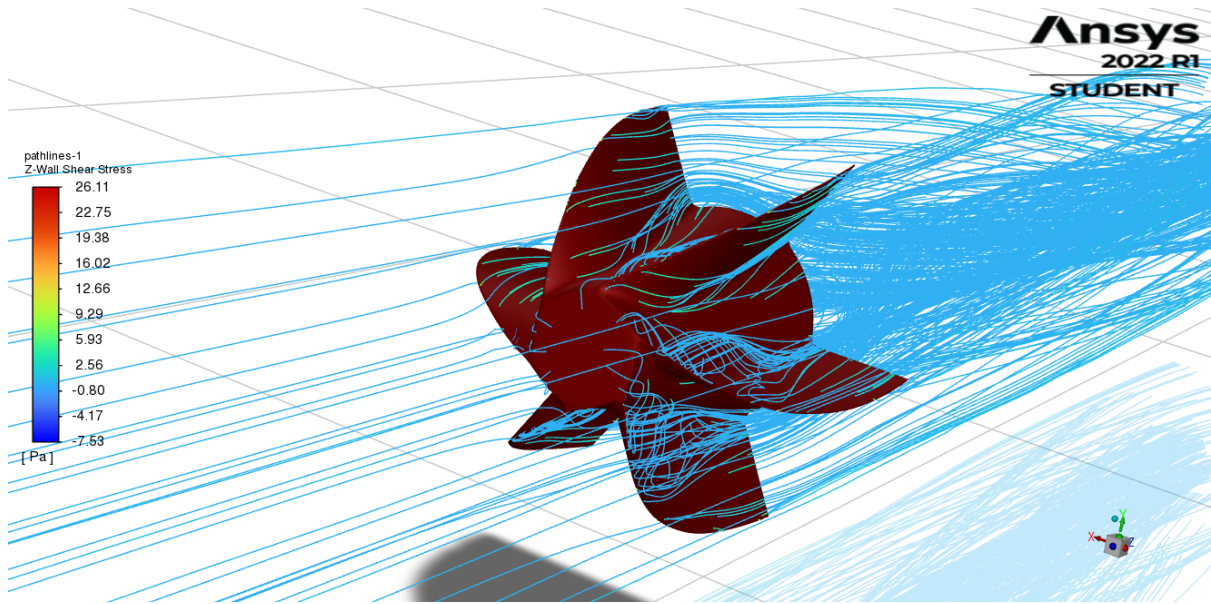


Figure 21 Pathlines of Z – Wall Shear Stress

Values of Y and Z – WSS are higher than those from the first simulation as expected.

Figure 22 shows the contours of Z-Wall Shear Stress on the surface of the impeller.

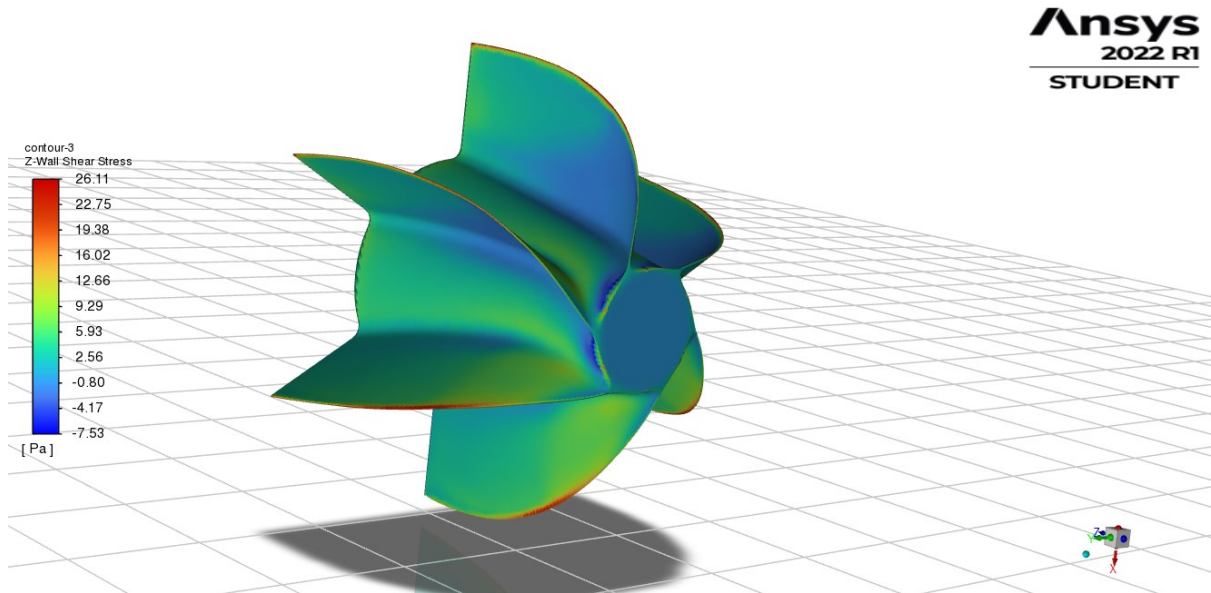


Figure 22 Contours of Z-WSS on the surface of the impeller

Figure 23 shows the profile of Z-WSS through the impeller as the X-Y plot.

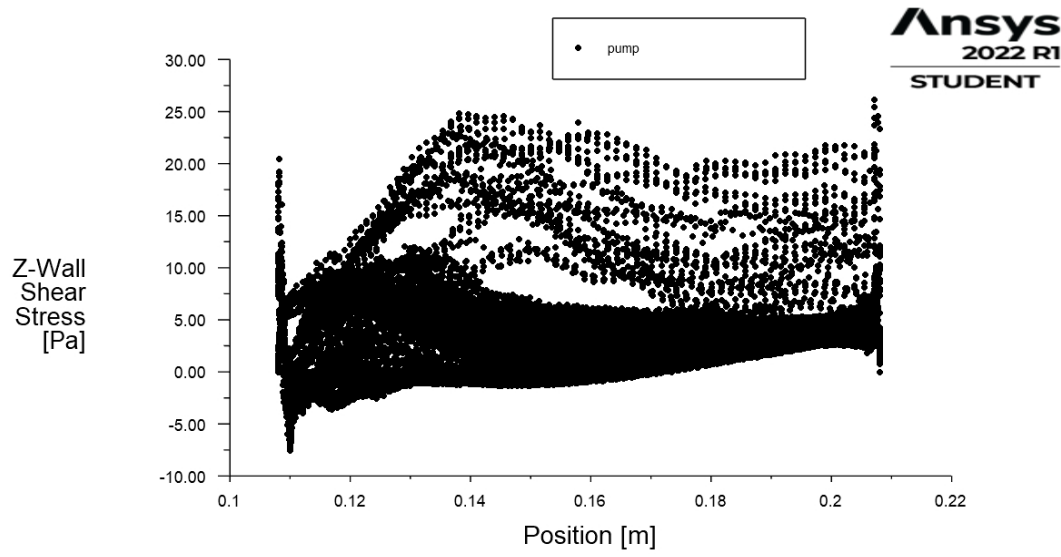


Figure 23 Characteristics of Z-WSS through the impeller

The results are the same as in the first simulation but values are almost two times bigger (as expected).

For different visual representation of the WSS, particle tracks simulation were done for YZ plane (as it is shown in figure 24).

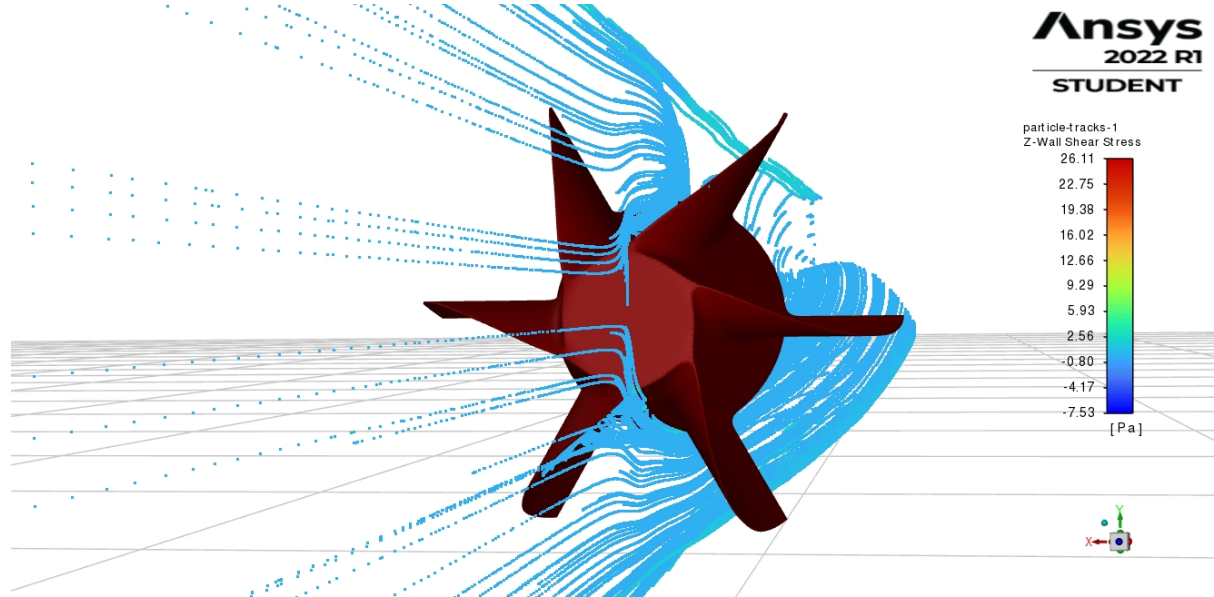


Figure 24 Particle traces in YZ plane for Z-WSS

Results of Z-WSS and Y-WSS for the YZ plane are as follows:

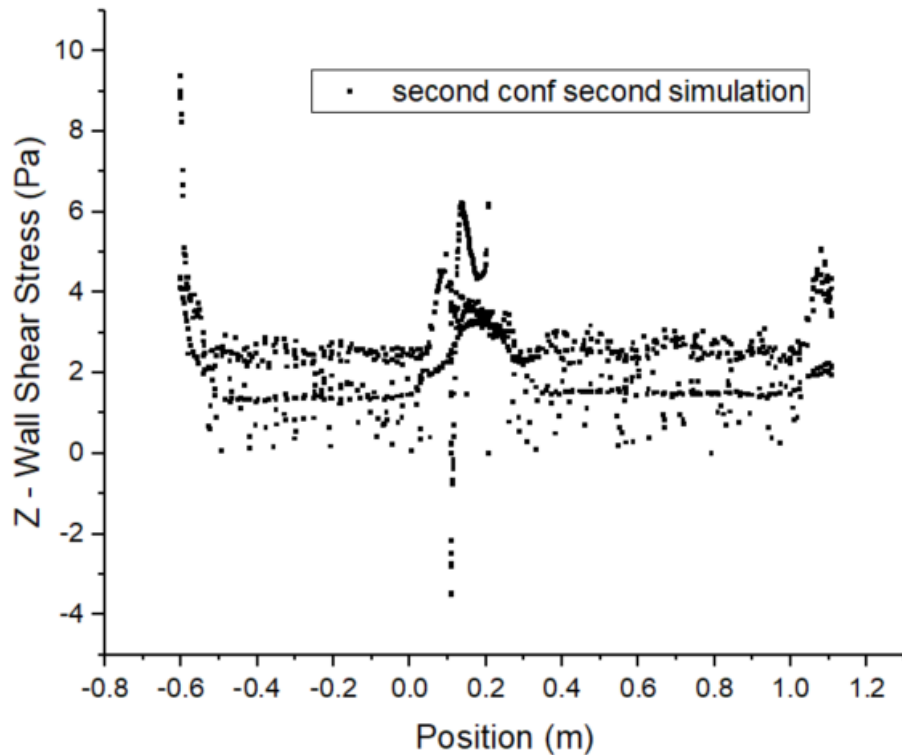


Figure 25 Z-WSS for YZ – plane (between blades)

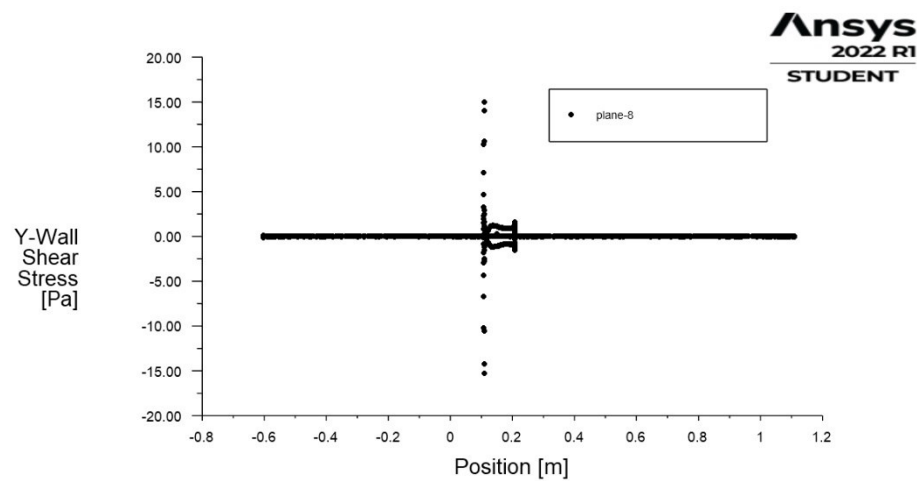


Figure 26 Y-WSS for YZ – plane (between blades)

Hydraulic resistance in this case yields:

$$R_H = \frac{\Delta p}{Q} = 2.31 * 10^{13} \frac{kg}{m^4 s}$$

3.1.3 COMPARISON

To summarize, comparison characteristic for Z-WSS through the impeller and for Z-WSS for YZ – plane (between blades) were made to visualize differences between two simulations, and also for validation.

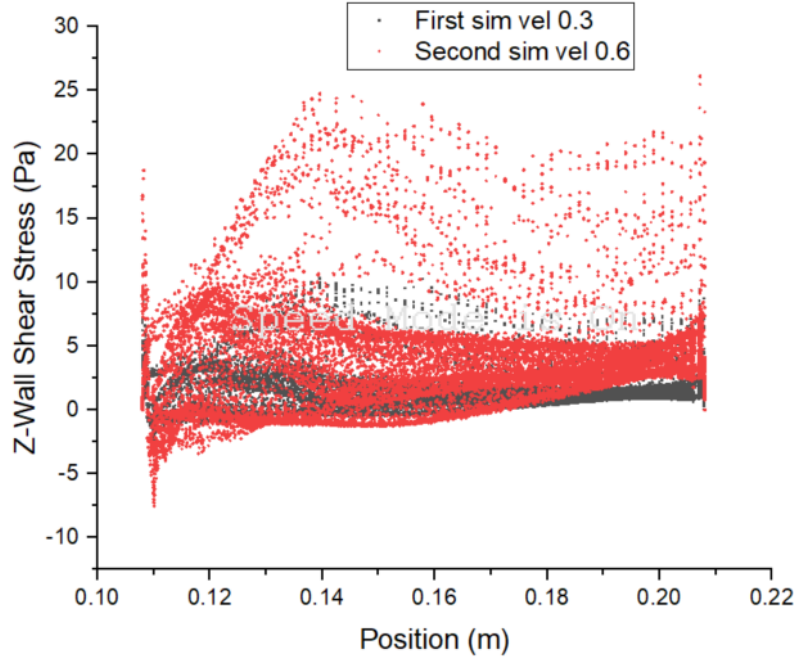


Figure 27 Characteristics of Z-WSS through the impeller for both simulations

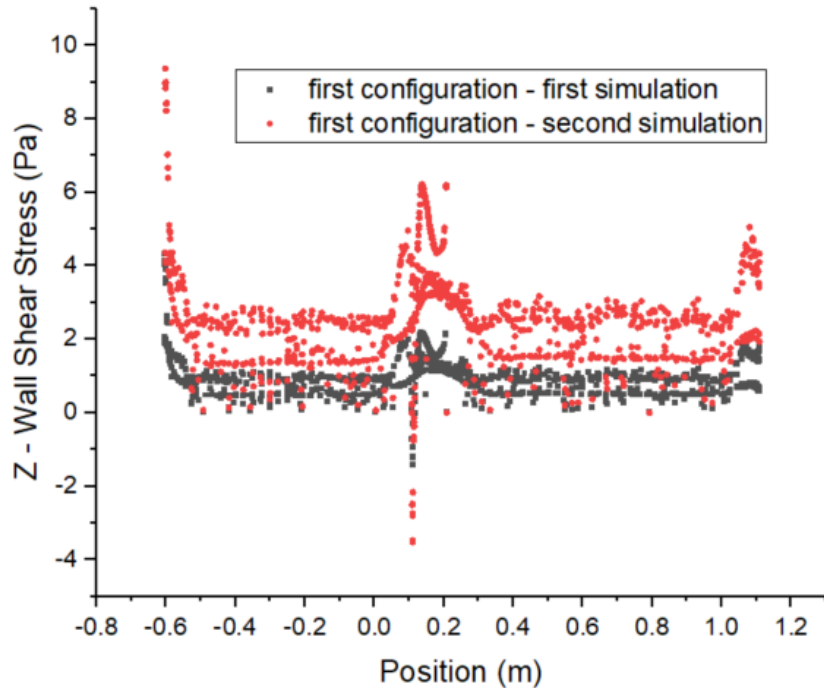


Figure 28 Characteristics of Z-WSS for YZ – plane (between blades) for both simulations.

3.2 SECOND CONFIGURATION

3.2.1 FIRST SIMULATION

First simulation was made for velocity inlet = 0.3 m/s. Value of density was taken as $\rho_{blood} = 1060 \text{ kg/m}^3$. As a viscous model the k-omega SST model was chosen. For pressure outlet – Gauge Pressure was set to 0 Pa. Impeller and pipe were set as a wall boundary. Simulation was set to Pressure-Based and Steady.

Figure 29 and 30 show the axial velocity (Z – velocity) before and after the impeller.

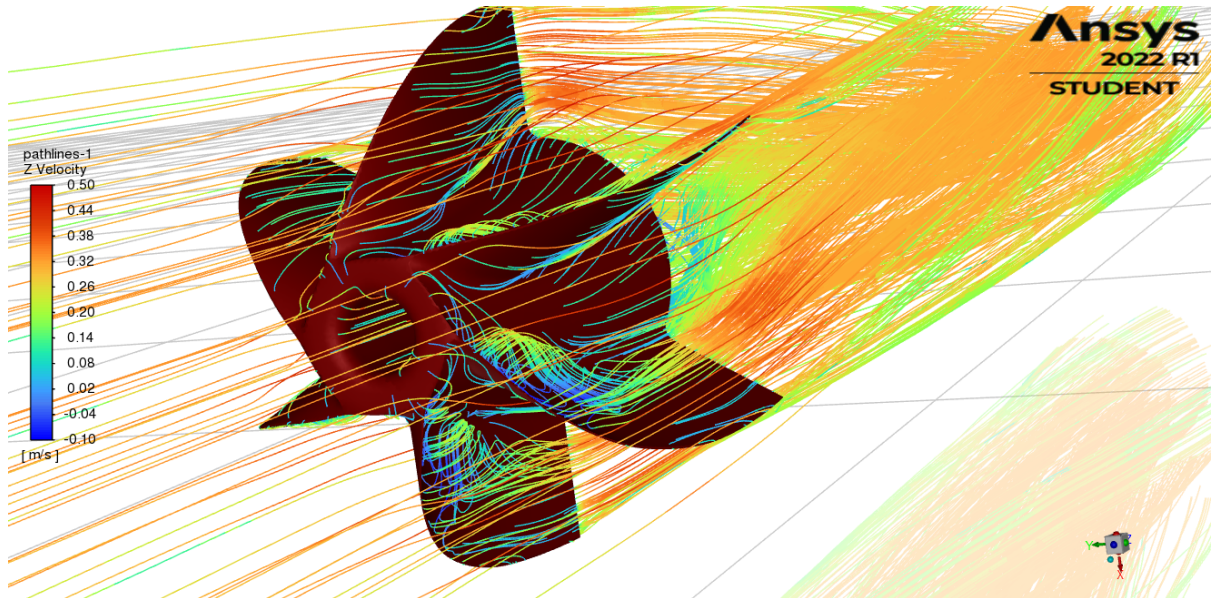


Figure 29 Axial velocity before the impeller

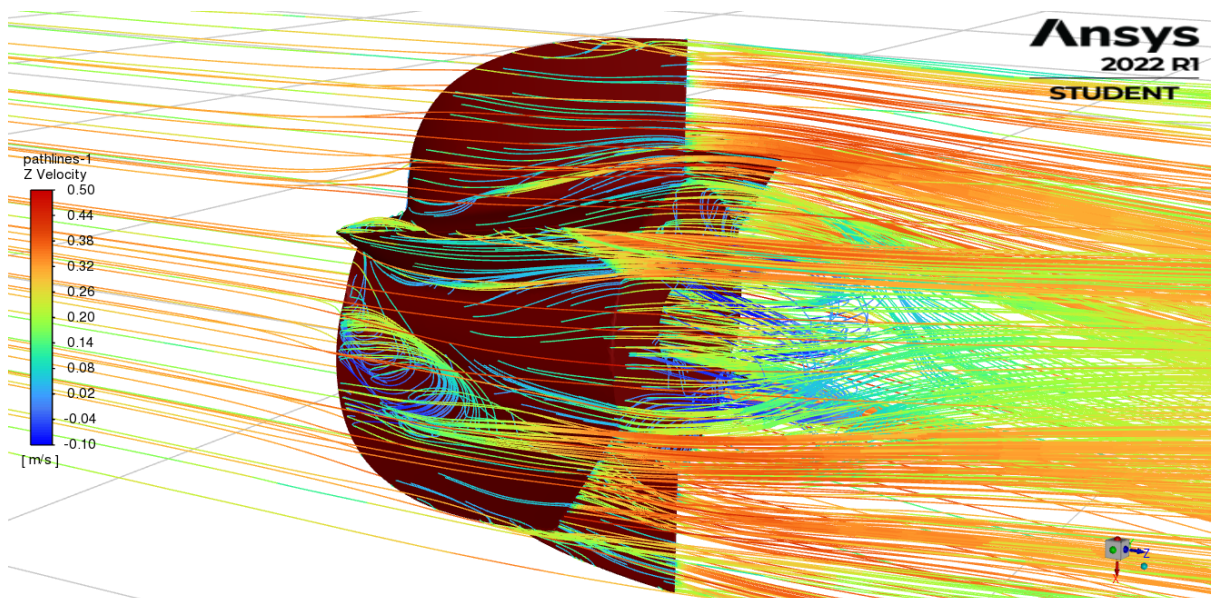


Figure 30 Axial velocity after the impeller

As in previous configuration there is a separation of flow (separation bubble), but due to the hole, it is considerably shorter (in axial direction), thus in terms of the optimization of the geometry (to prevent separation of the flow) impeller with a hole could be shorter (comparing to the geometry without a hole).

Phenomena at the leading edge of the blades are similar to those in the first configuration, therefore conclusions in that matter are the same.

Figure 31 shows the velocity vectors (velocity magnitude) for a flow through a pipe.

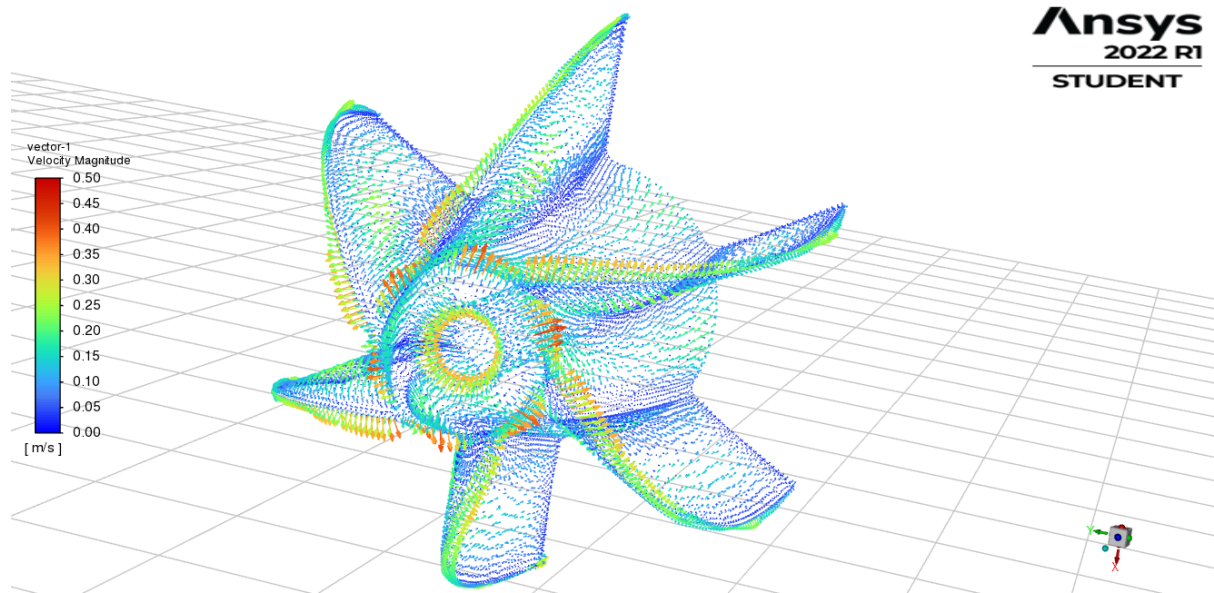


Figure 31 Velocity vectors – velocity magnitude

Due to the hole, area that stops flow of the blood is significantly smaller comparing to the first configuration, thus smaller values of the WSS are expected.

Figure 32 and figure 33 show pathlines of Y – Wall Shear Stress, and Z – Wall Shear Stress for the analysed flow.

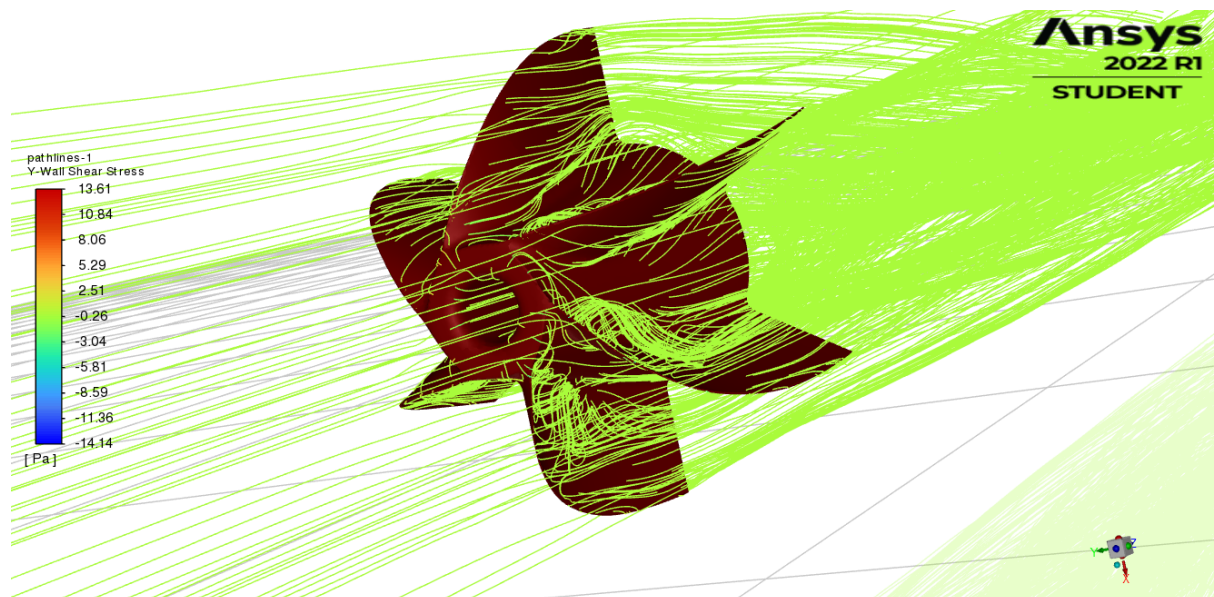


Figure 32 Pathlines of Y – Wall Shear Stress

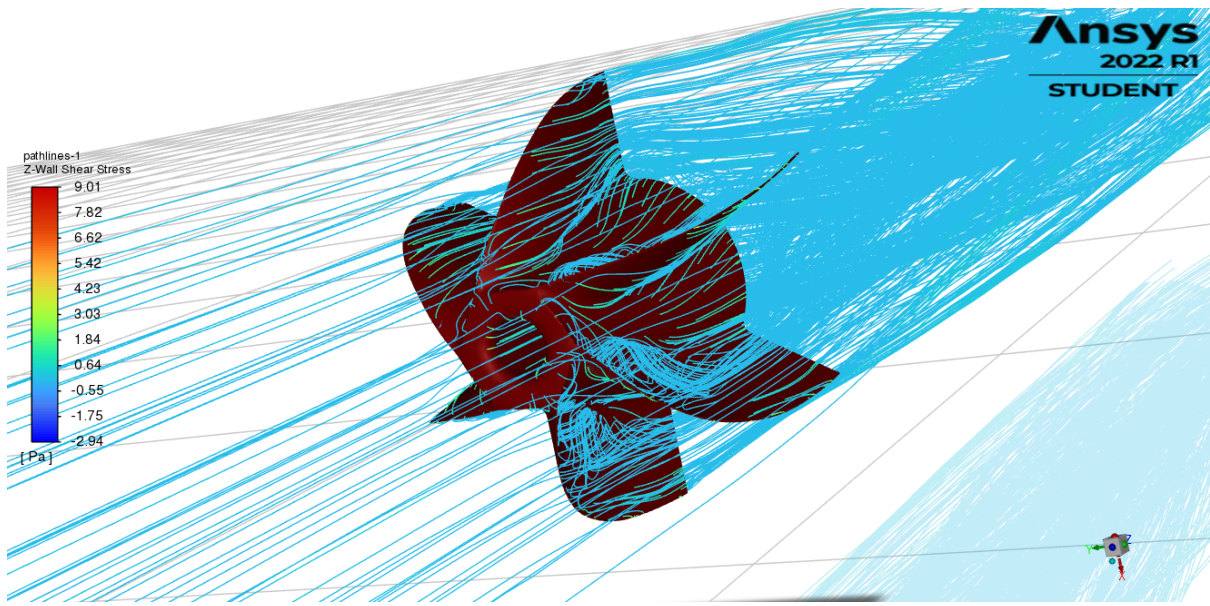


Figure 33 Pathlines of Z – Wall Shear Stress

Due to the rotation of the impeller values of Y – WWS are higher than for the axial Z-WSS.

Figure 34 shows contours of the Z – Wall Shear Stress on the surface of the impeller.

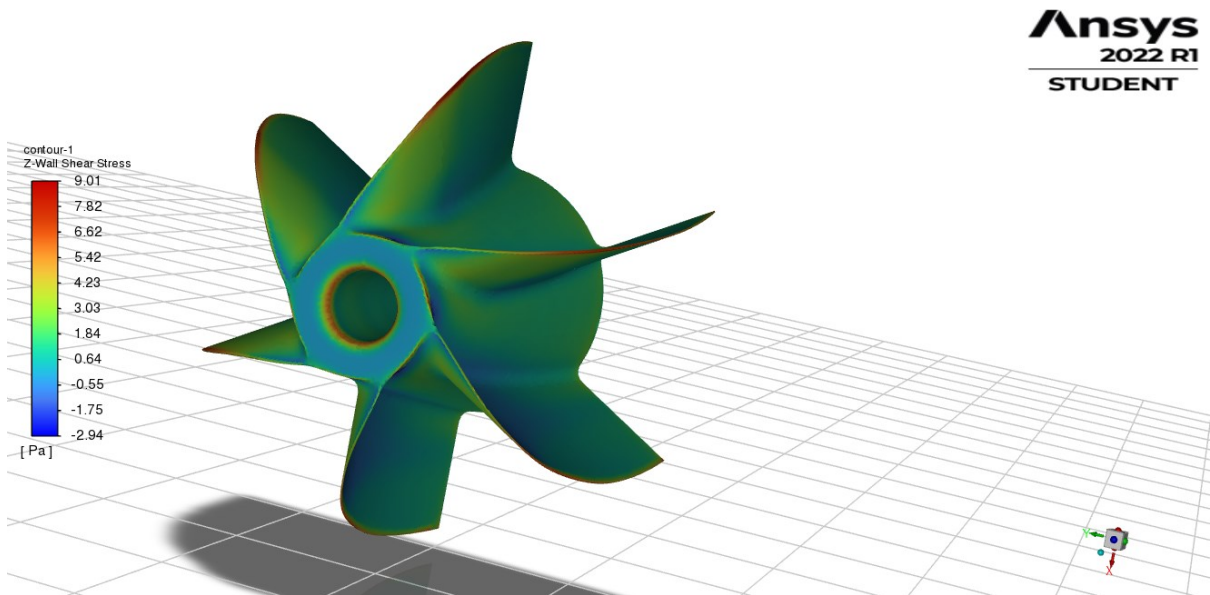


Figure 34 Contours of Z – WSS on the surface of the impeller

The highest value of the Z – WSS are obtained on the leading edge of the blades. As it was expected, due to the hole application in the centre of the impeller, value of the WSS decreased.

Figure 35 shows the profile of the Z – WSS through the impeller as the X – Y plot.

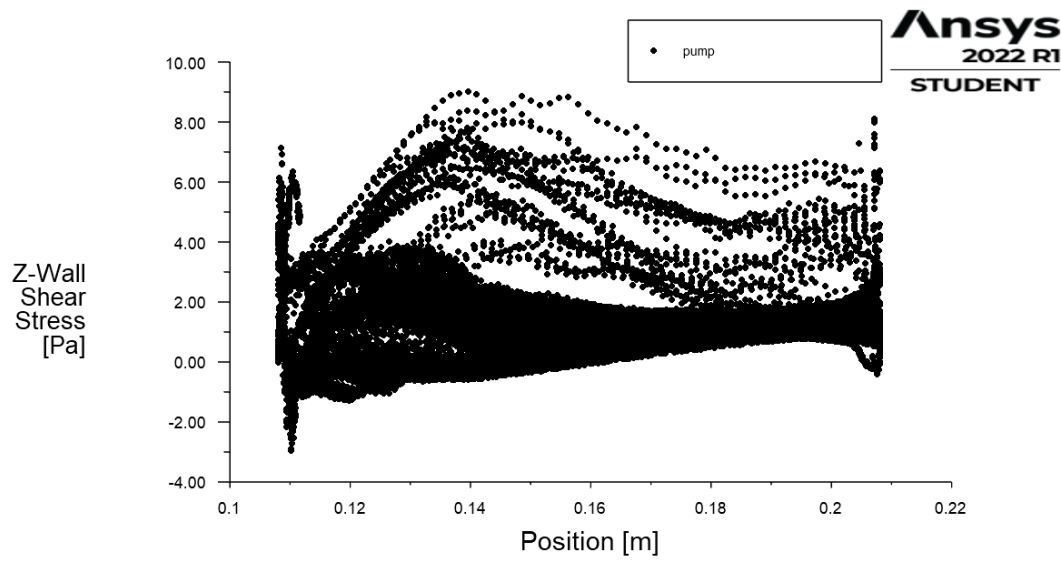


Figure 35 Characteristics of Z-WSS through the impeller

Two peaks of the Z-WSS can be observed, namely at the front face of the impeller and the back of the impeller, mostly due to the lack of the continuity of the geometry, therefore for further optimization modifications in those areas are desirable.

For different visual representation of the WSS, particle tracks simulation were done for YZ plane (as it is shown in figure 35).

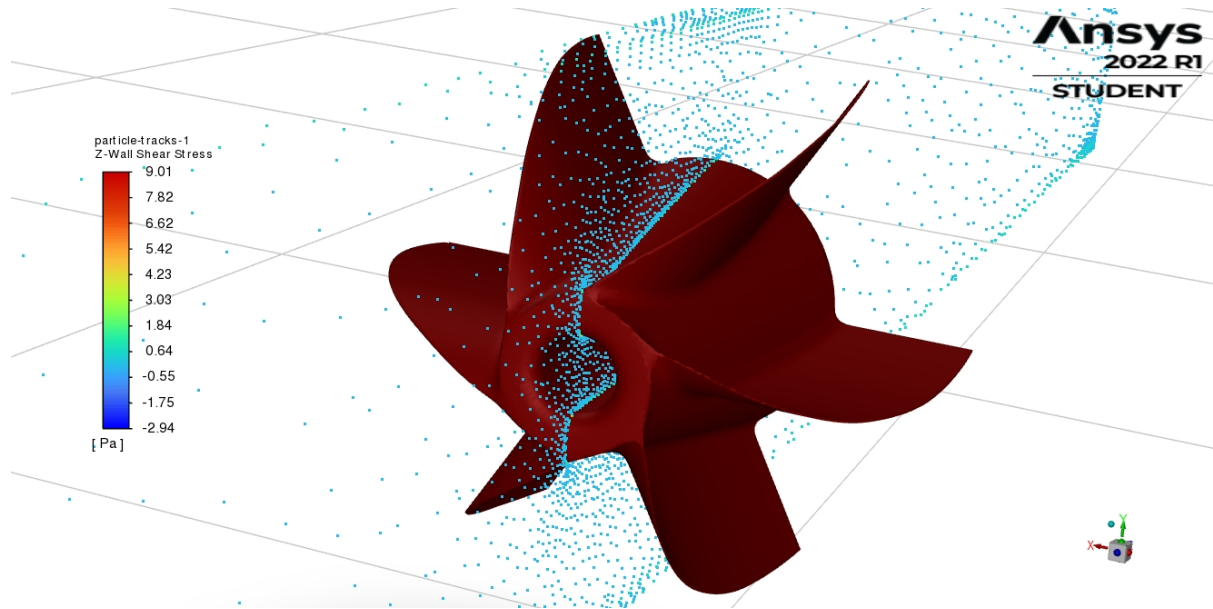


Figure 36 Particle traces on YZ plane for Z - WSS

For the above plane the following results of Z-WSS and Y-WSS were obtained.

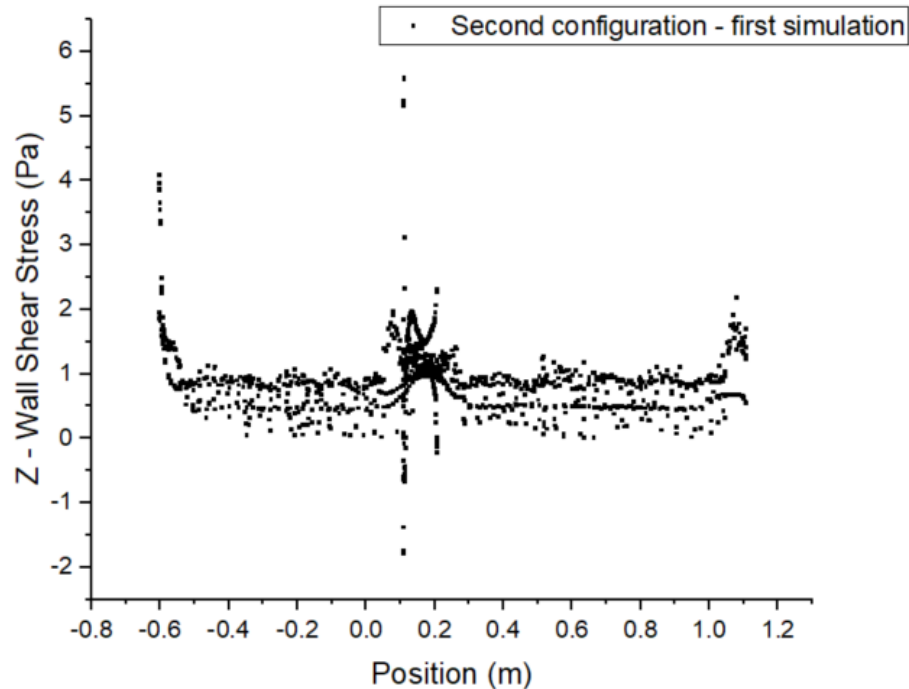


Figure 37 Z – WSS for YZ – plane (between blades)

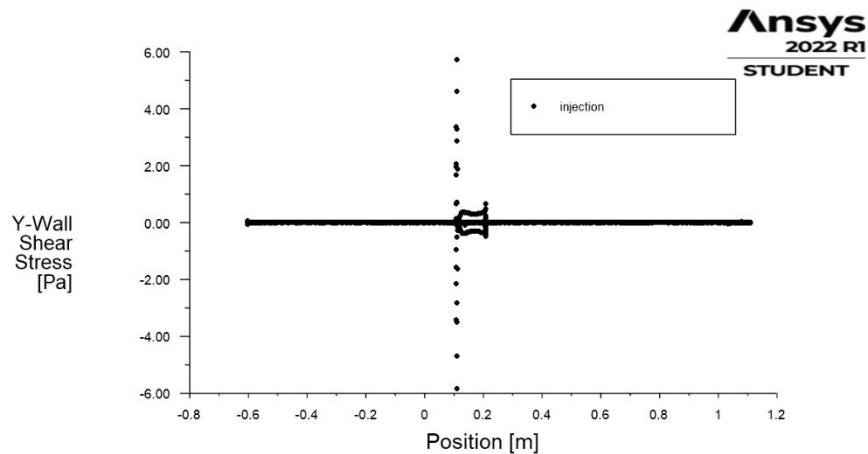


Figure 38 Y – WSS for YZ – plane (between blades)

Hydraulic Resistance:

$$R_H = \frac{\Delta p}{Q} = 9.53 * 10^{11} \frac{kg}{m^4 s}$$

3.2.2 SECOND SIMULATION

In order to validate the results from the first simulation, second simulation was made. The only change was made for the inlet velocity = 0.6 m/s (higher velocity value – higher values of WSS are expected).

Figure 39 and 40 show the axial velocity (Z – velocity) before and after the impeller.

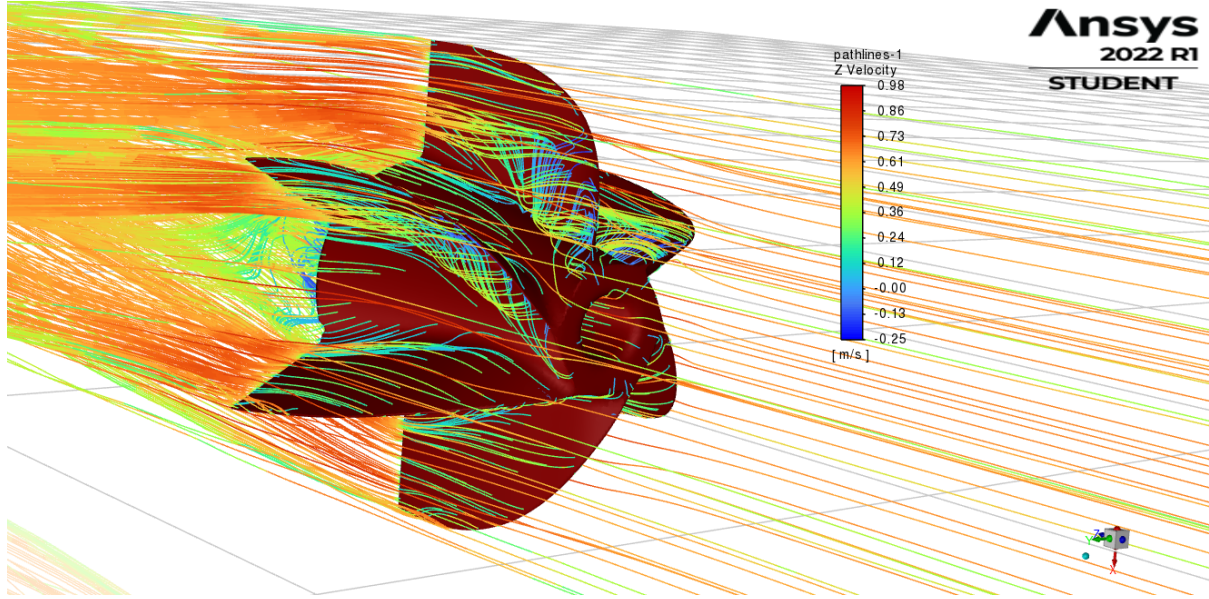


Figure 39 Axial velocity - before the impeller

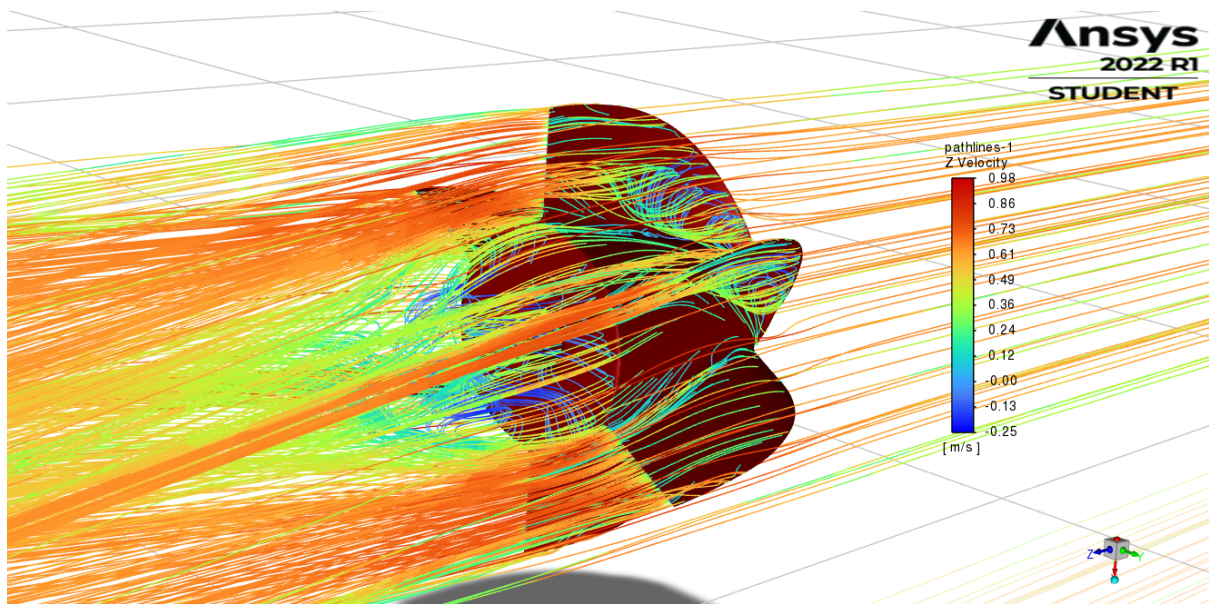


Figure 40 Axial velocity - after the impeller

The phenomena are the same as in the first simulation and, as expected values of velocity are higher.

Figure 41 shows the velocity vectors (velocity magnitude) for a flow through a pipe.

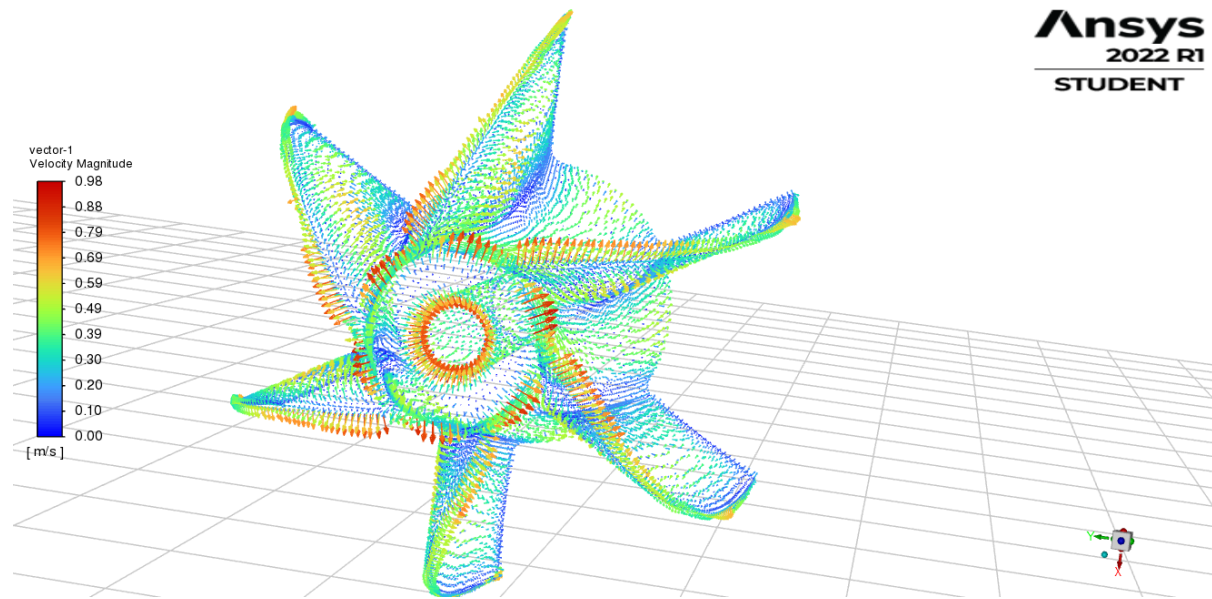


Figure 41 Velocity vectors – velocity magnitude

Figure 42 and 43 show pathlines of Y – WSS, and Z – WSS for the analysed flow.

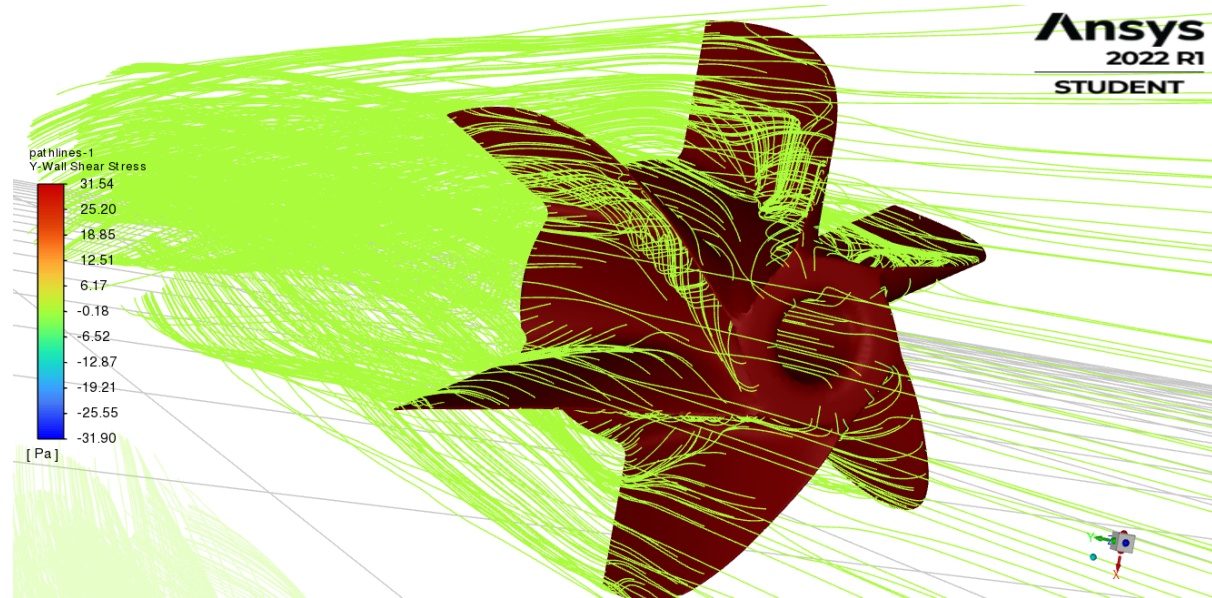


Figure 42 Pathlines of Y – WSS

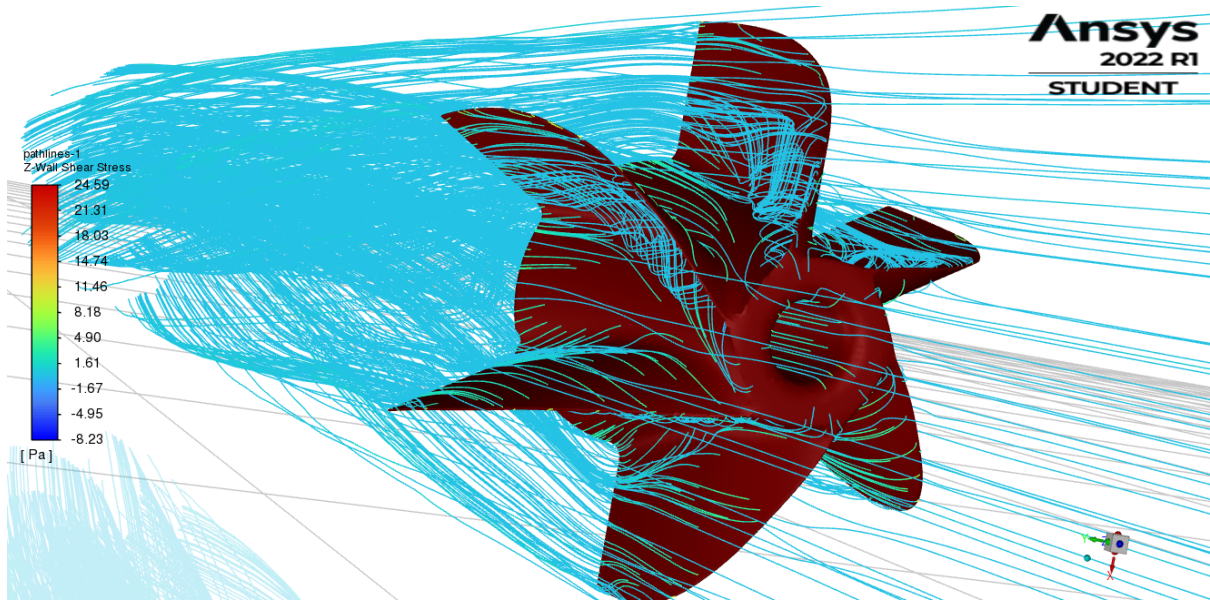


Figure 43 Pathlines of Z – WSS

Values of Y and Z – WSS are higher than those from the first simulation as expected.

Figure 44 shows the contours of Z – WSS on the surface of the impeller.

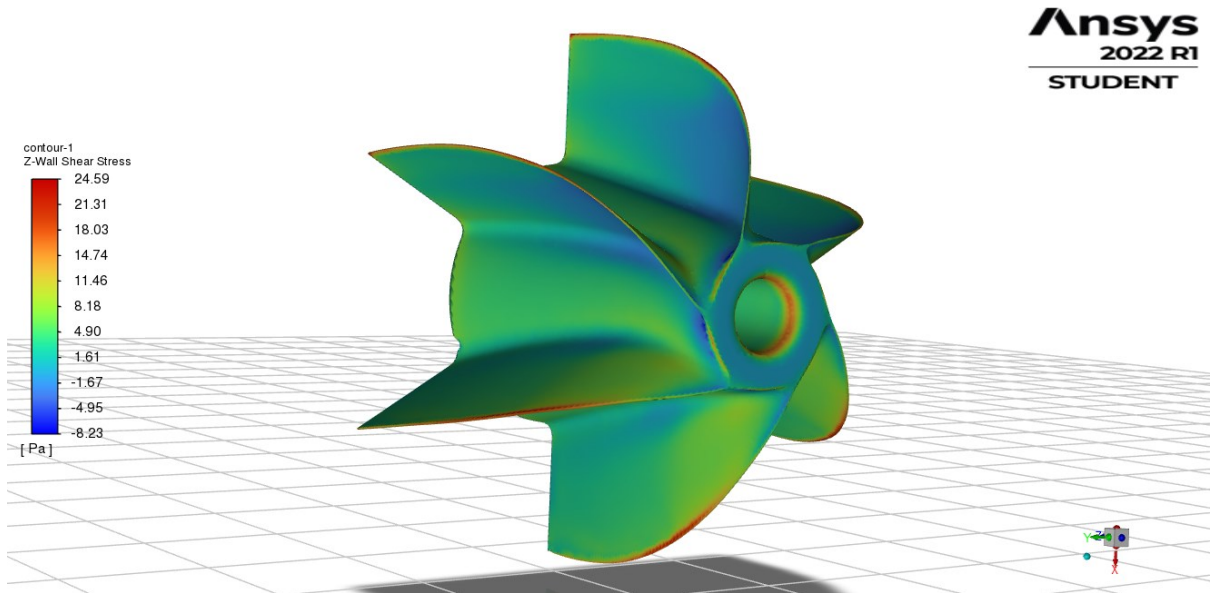


Figure 44 Contours of Z – WSS on the surface of the impeller

Figure 45 shows the profile of Z – WSS through the impeller as the X-Y plot.

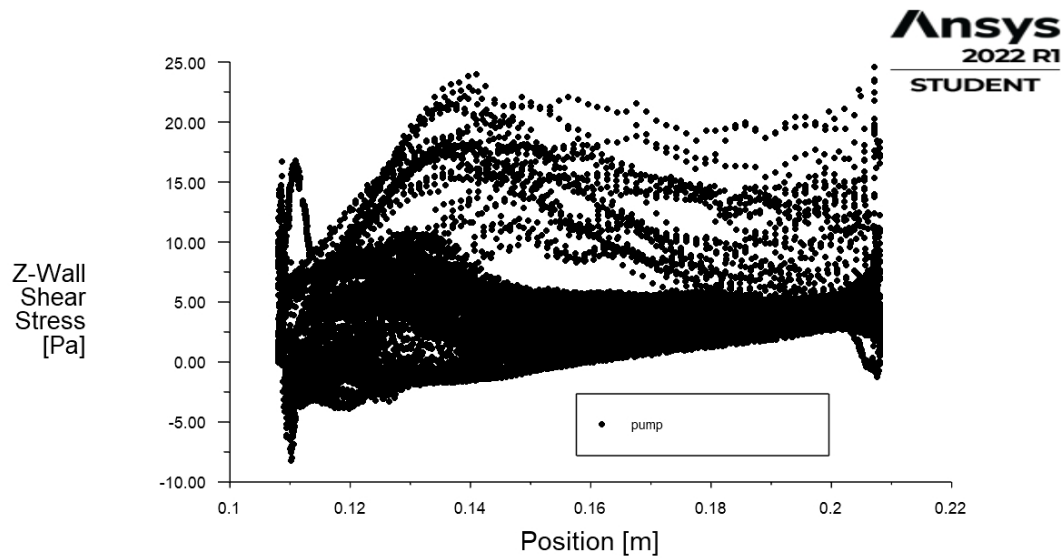


Figure 45 Characteristics of Z – WSS through the impeller

The results are the same as in the first simulation but values are almost two times bigger (as expected).

For different visual representation of the WSS, particle tracks simulation were done for YZ plane (as it is shown in figure 46).

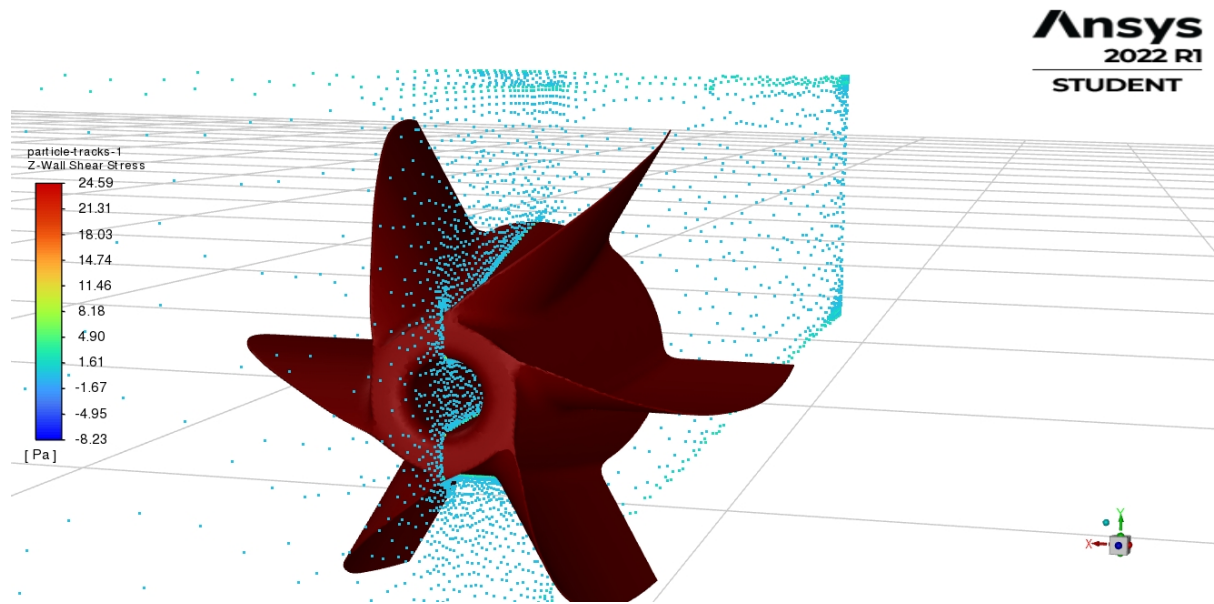


Figure 46 Particle traces on the YZ plane for Z-WSS

Results of Z-WSS and Y-WSS for the YZ plane are as follows:

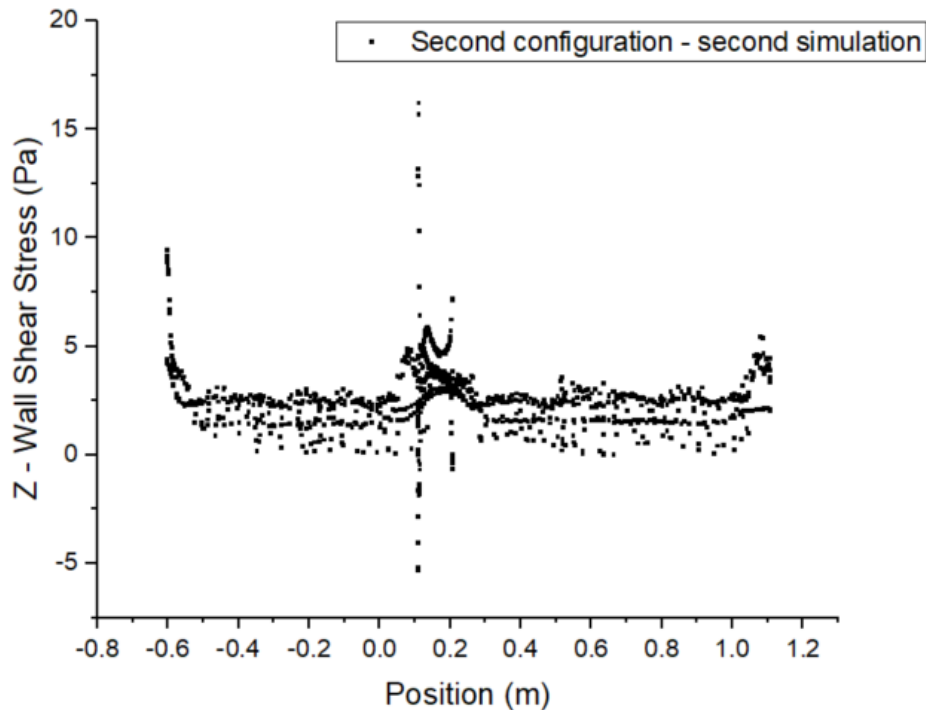


Figure 47 Z-WSS for YZ – plane (between blades)

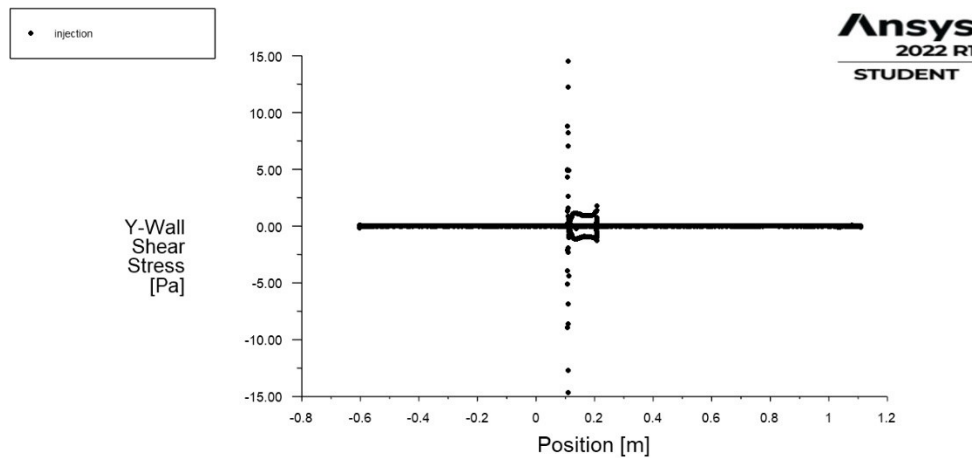


Figure 48 Y – WSS for YZ – plane (between blades)

Hydraulic resistance in this case yields:

$$R_H = \frac{\Delta p}{Q} = 2.15 * 10^{12} \frac{kg}{m^4 s}$$

3.2.3 COMPARISON

To summarize, comparison characteristic for Z-WSS through the impeller and for Z-WSS for YZ – plane (between blades) were made to visualize differences between two simulations, and also for validation.

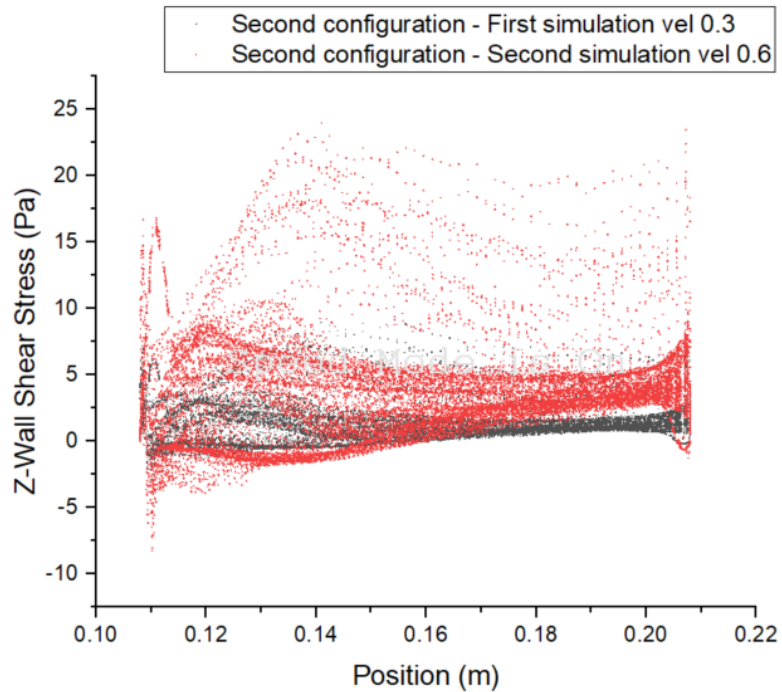


Figure 49 Characteristics of Z-WSS through the impeller for both simulations

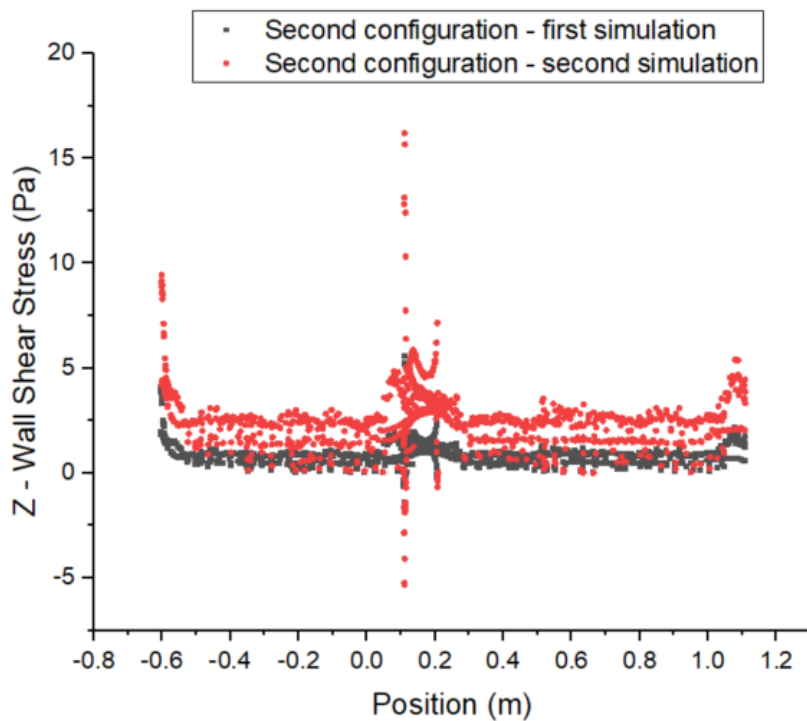


Figure 50 Characteristics of Z-WSS for YZ – plane (between blades) for both simulations.

3.3 THIRD CONFIGURATION

3.3.1 FIRST SIMULATION

First simulation was made for velocity inlet = 0.3 m/s. Value of density was taken as $\rho_{blood} = 1060 \text{ kg/m}^3$. As a viscous model the k-omega SST model was chosen. For pressure outlet – Gauge Pressure was set to 0 Pa. Impeller and pipe were set as a wall boundary. Simulation was set to Pressure-Based and Steady.

Figure 51 and 52 show the axial velocity (Z – velocity) before and after the impeller.

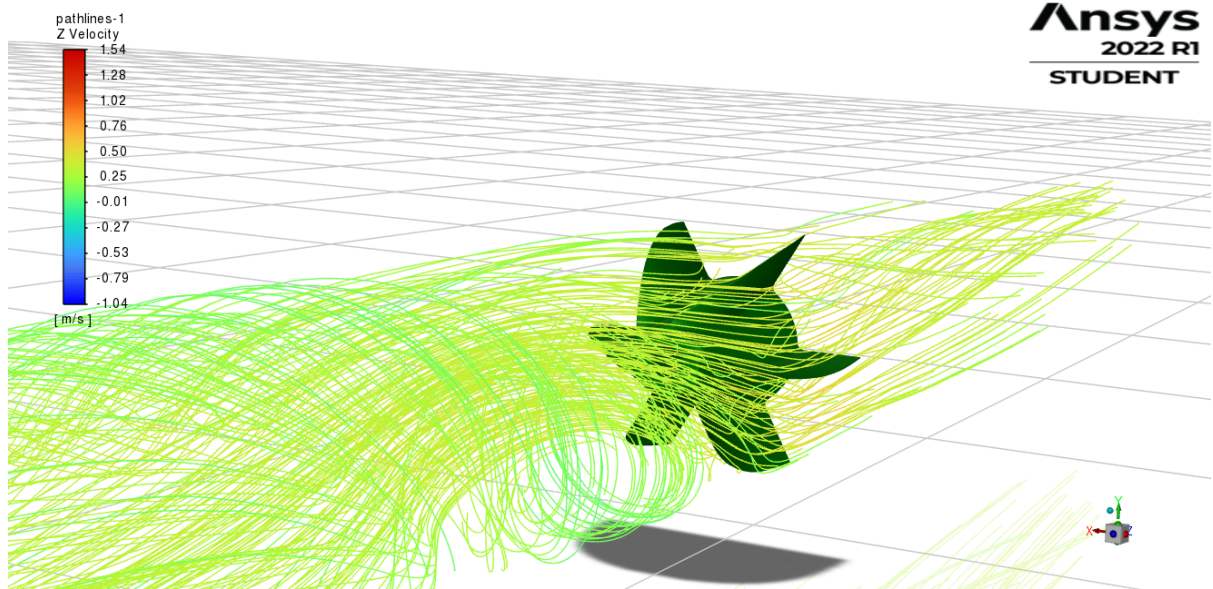


Figure 51 Axial velocity before the impeller

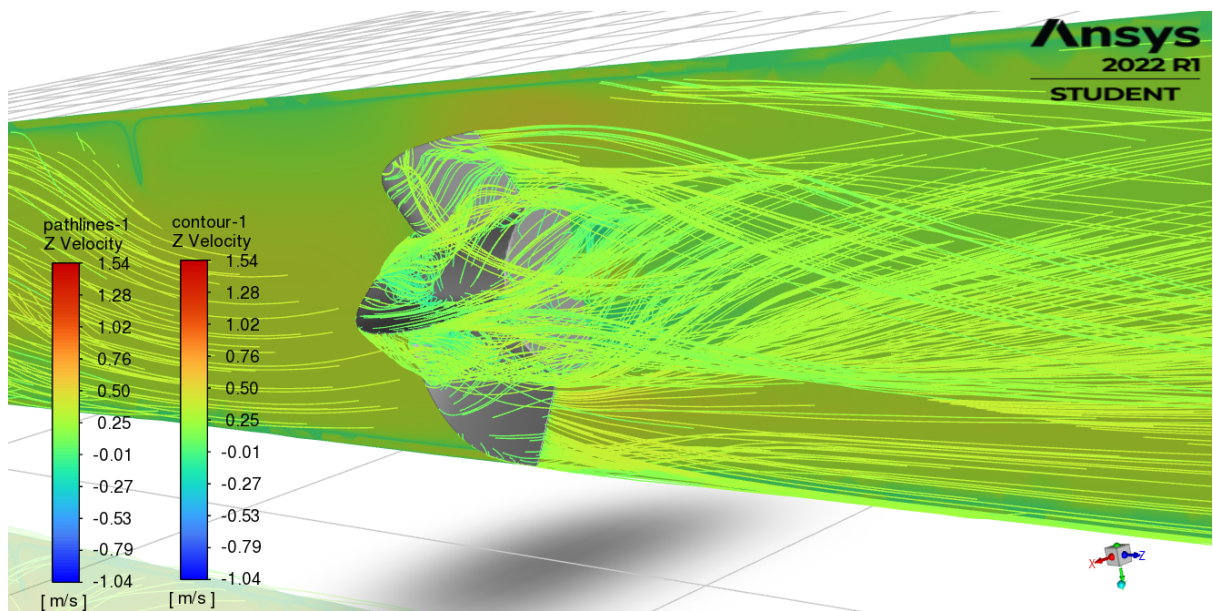


Figure 52 Axial velocity after the impeller

Due to the initial eddy in the flow higher vorticity after the impeller is occurred. That could be the cause of smaller size of the separation bubble after the impeller. Although, the size of the separation of the flow, value of axial velocity increases.

Figure 53 and 54 show the velocity vectors (velocity magnitude) for a flow through a pipe.

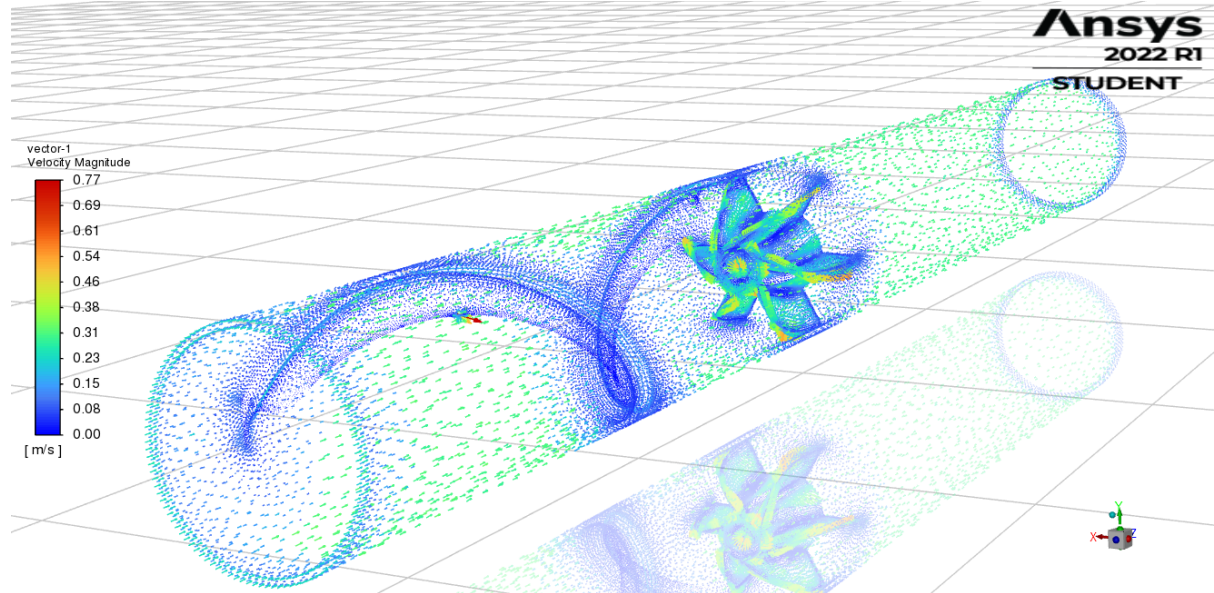


Figure 53 Velocity vectors – velocity magnitude

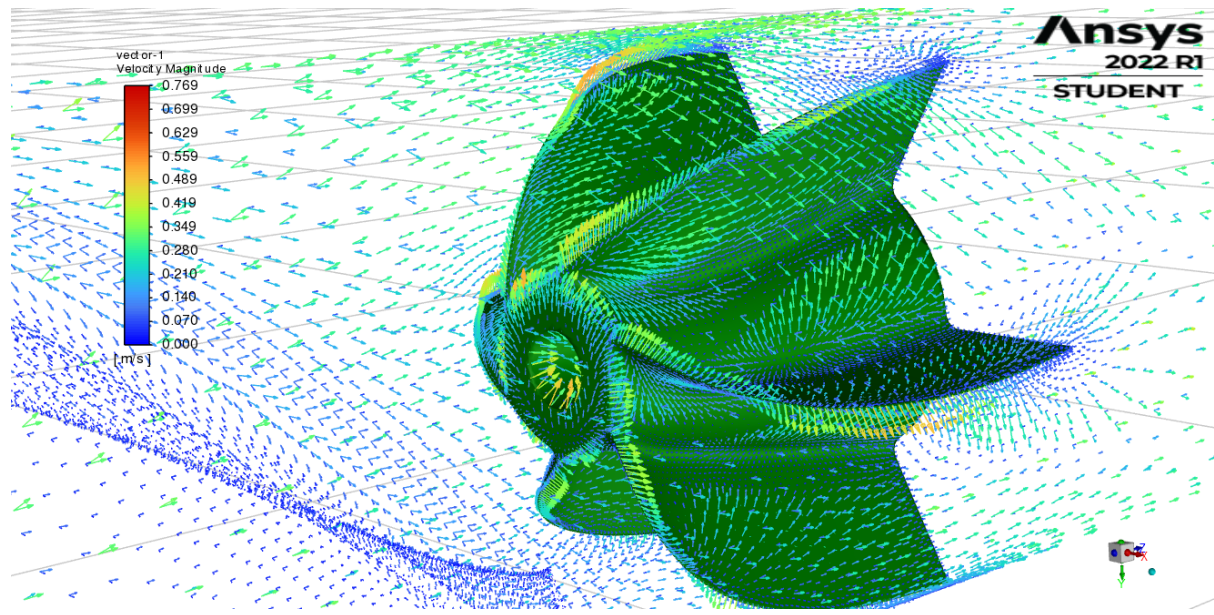


Figure 54 Velocity vectors – velocity magnitude

Figure 55 and 56 show pathlines of Y – WSS and Z – WSS for the analysed flow.

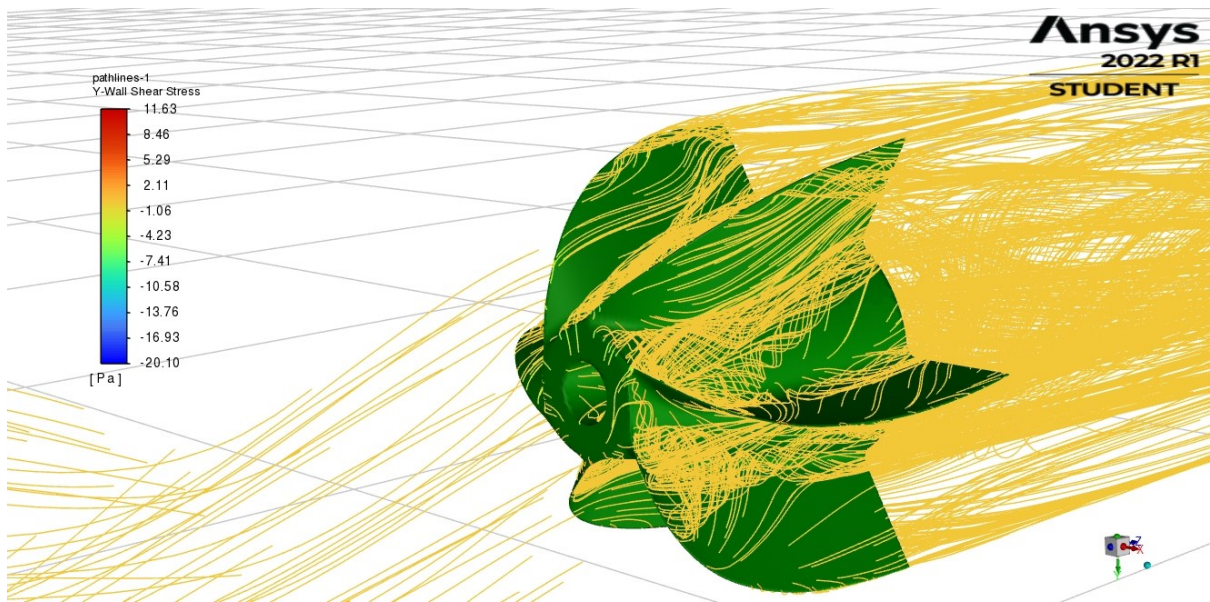


Figure 55 Pathlines of Y – WSS

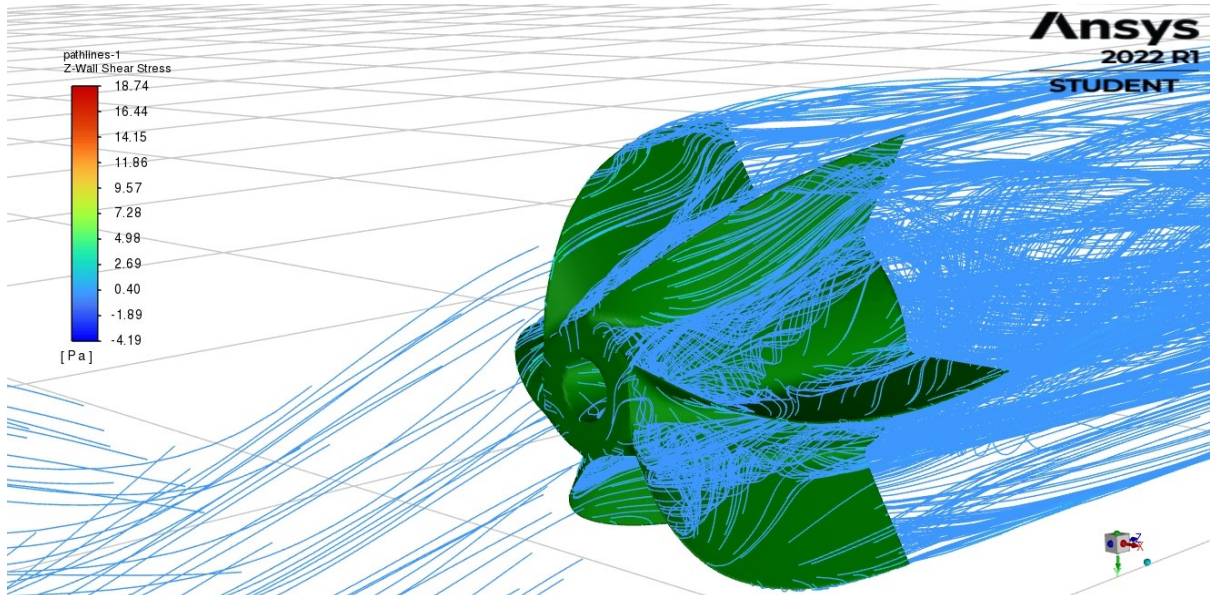


Figure 56 Pathlines of Z – WSS

In this particular configuration, comparing to the second one, the maximum value of Y-WSS is smaller, whereas the maximum value of the Z-WSS is significantly bigger.

Figure 57 shows contours of the Z – WSS on the surface of the impeller.

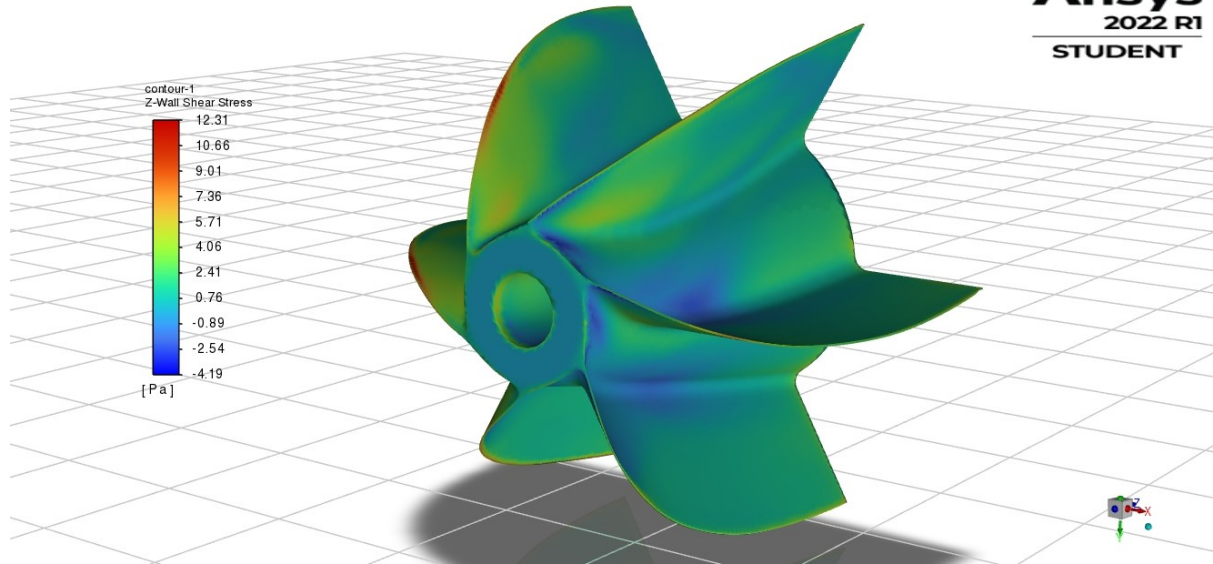


Figure 57 Contours of Z – WSS on the surface of the impeller

The highest value of the Z – WSS are obtained on the leading edge of the blades. The highest value of Z-WSS for a pump is smaller than for the whole pipe thus modification of the geometry before the impeller increases the value of Z - WSS.

Figure 58 shows the profile of the Z – WSS through the impeller as the X-Y plot.

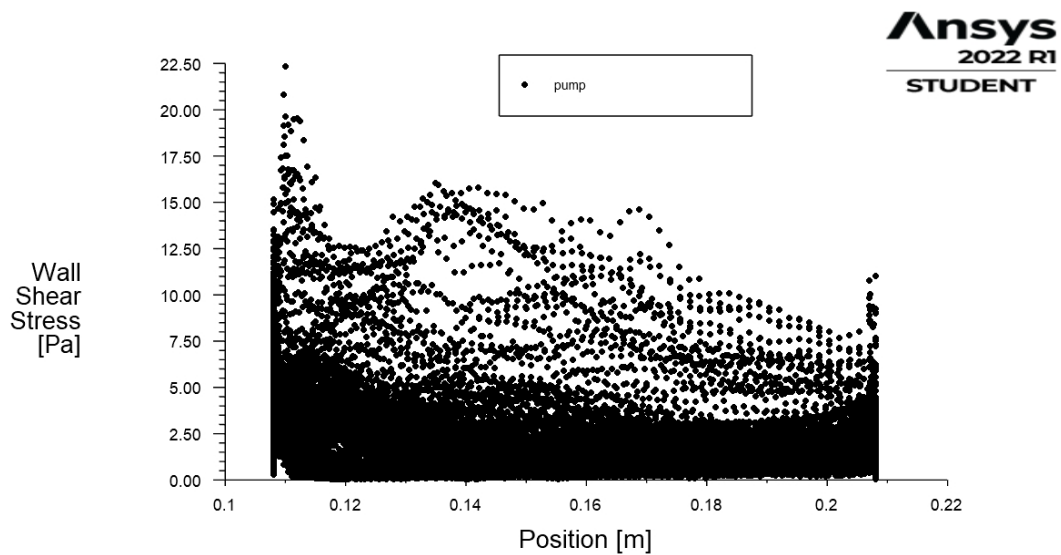


Figure 58 Characteristics of Z – WSS through the impeller

The results of the Z-WSS for the profile of the impeller are higher than for the second configuration.

For different visual representation of the WSS, particle tracks simulation were done for YZ plane (as it is shown in figure 59).

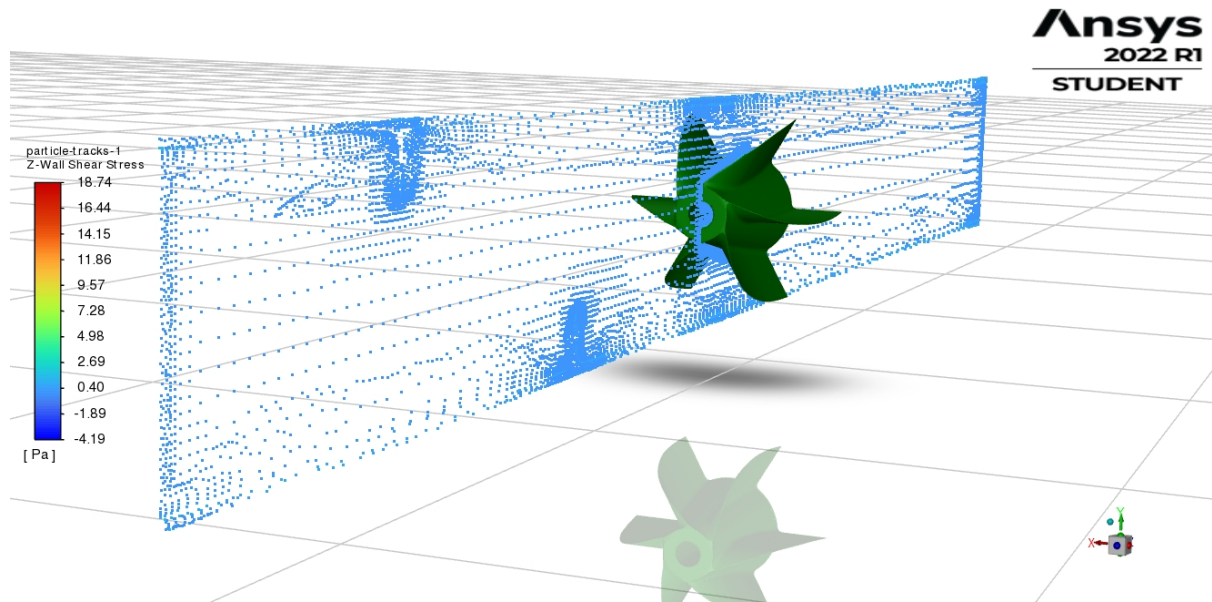


Figure 59 Particle traces on YZ plane for Z – WSS

For the YZ plane the following results of Z-WSS and Y-WSS were obtained.

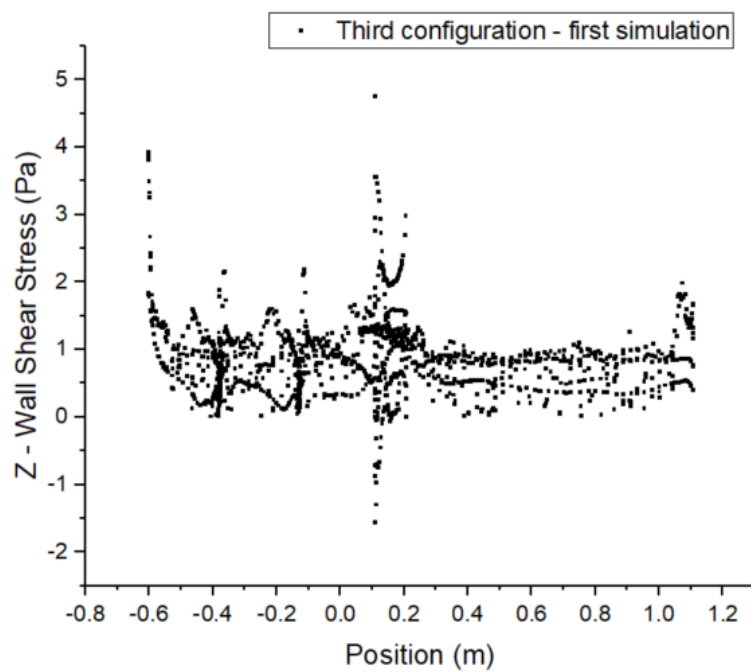


Figure 60 Z -WSS for YZ – plane (between blades)

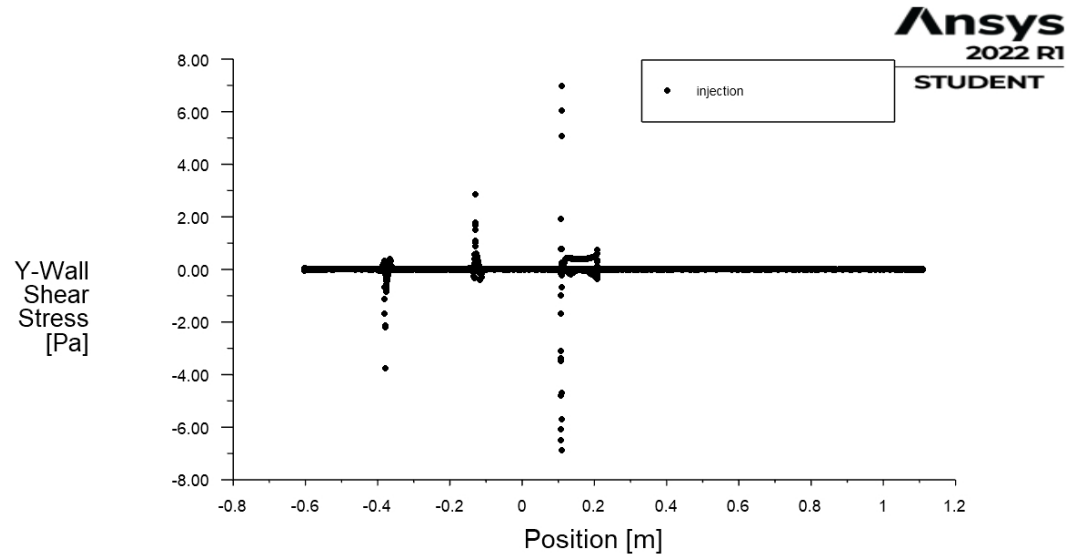


Figure 61 Y-WSS for YZ – plane (between blades)

For Y-WSS three peaks can be observed due to the dramatic change in the geometry of the pipe (application of airfoil at the inner surface of the pipe for initial rotational movement of the blood before the impeller).

Hydraulic Resistance:

$$R_H = \frac{\Delta p}{Q} = 1.5 * 10^{12} \frac{kg}{m^4 s}$$

3.3.2 SECOND SIMULATION

In order to validate the results from the first simulation, second simulation was made. The only change was made for the inlet velocity = 0.6 m/s (higher velocity value – higher values of WSS are expected).

Figure 62 - 64 show the axial velocity (Z – velocity) before, after the impeller, and behavior of fluid near to the airfoil area.

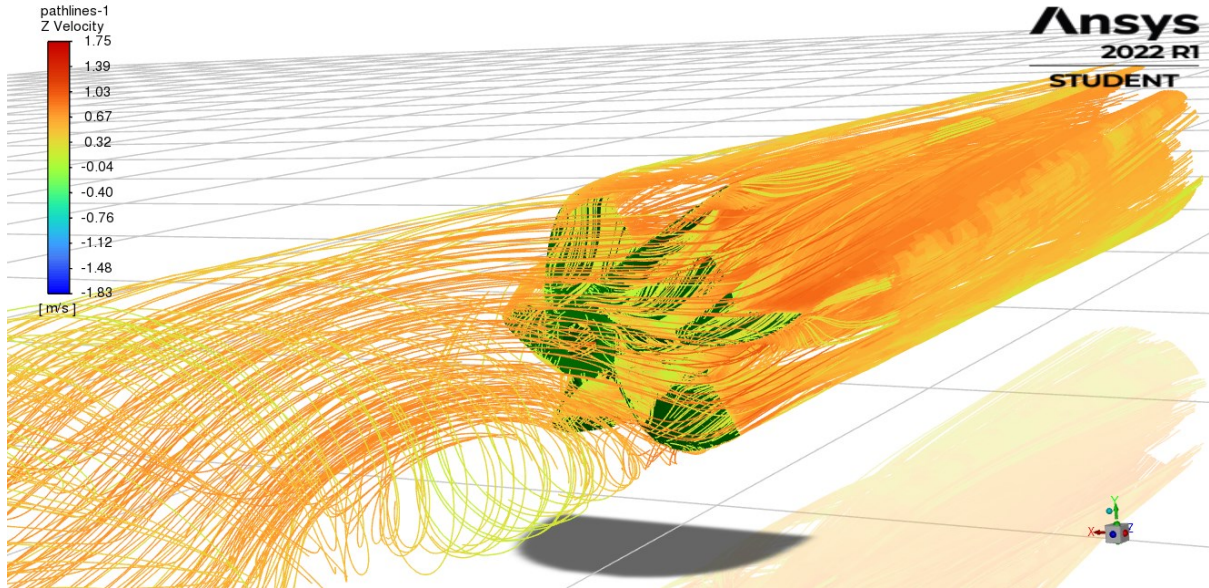


Figure 62 Axial velocity – before the impeller

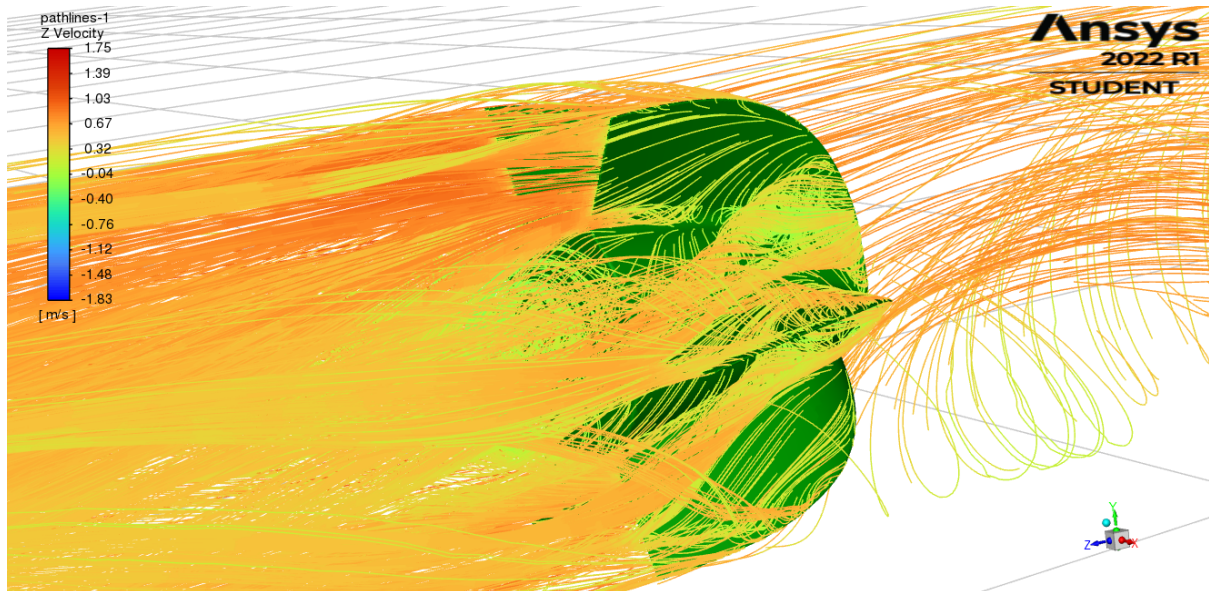


Figure 63 Axial velocity – after the impeller

The phenomena are the same as in the first simulation and, as expected values of velocity are higher.

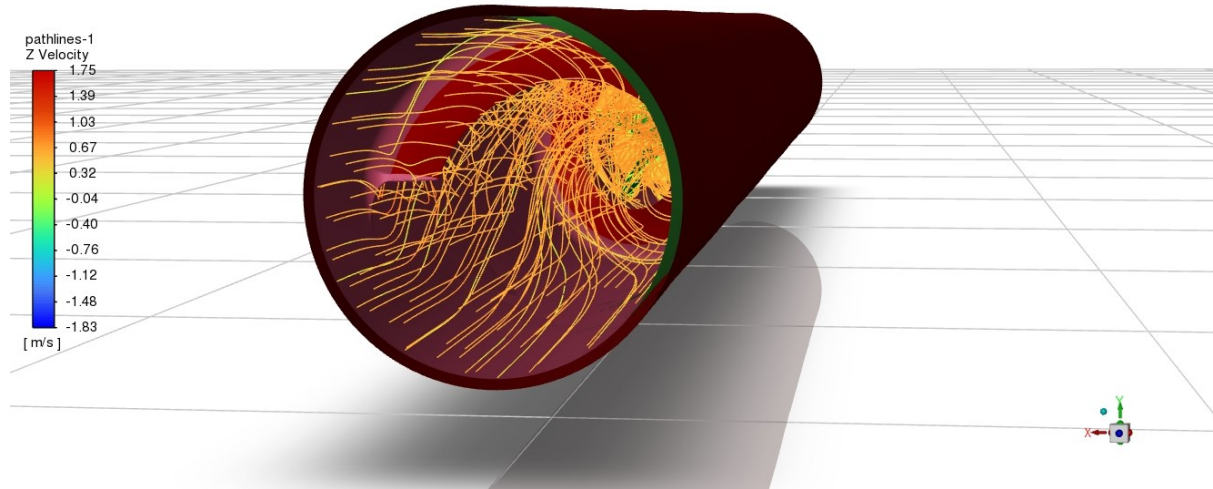


Figure 64 Axial velocity – behaviour of the blood flowing through spiral geometry with airfoil cross-section

In the figure 64 flow separation occurs, thus higher pitch of the helix is needed for the elimination of the flow separation.

Figure 65 shows the velocity vectors (velocity magnitude) for a flow through the pipe.

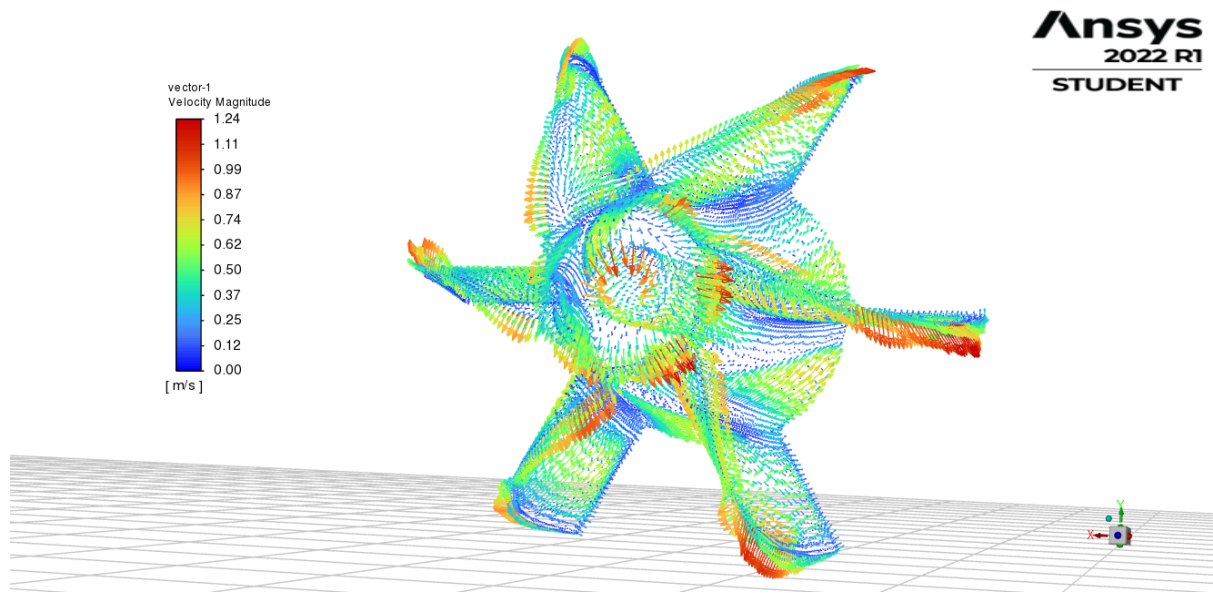


Figure 65 Velocity vectors – velocity magnitude

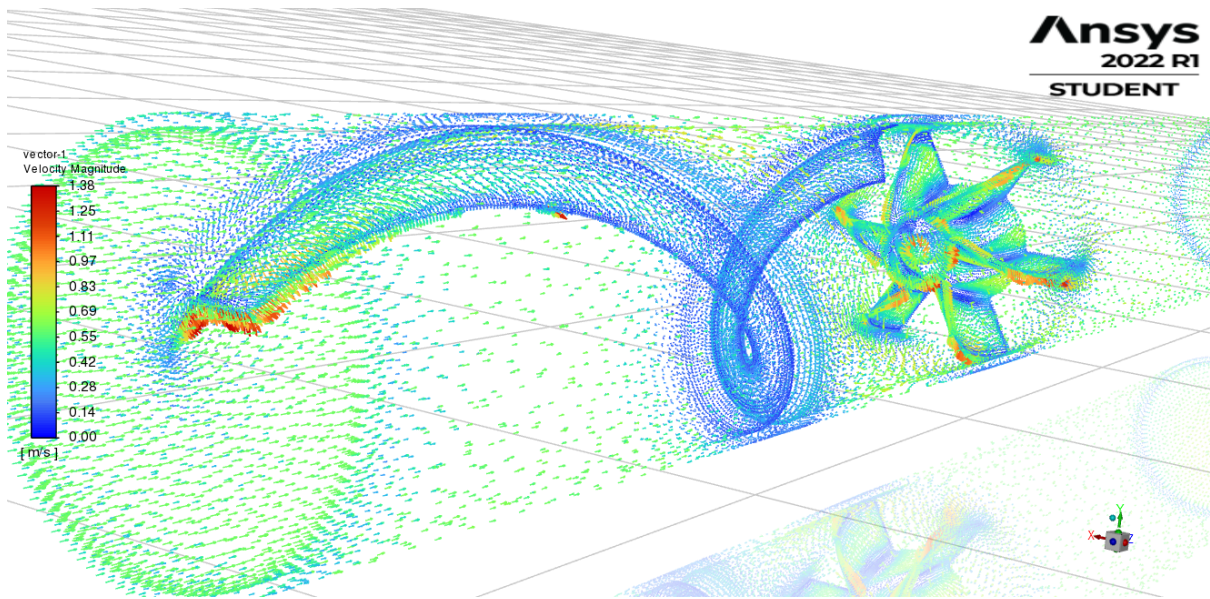


Figure 66 Velocity vectors – velocity magnitude

Figure 67 and 68 show pathlines of Y-WSS, and Z-WSS for the analysed flow.

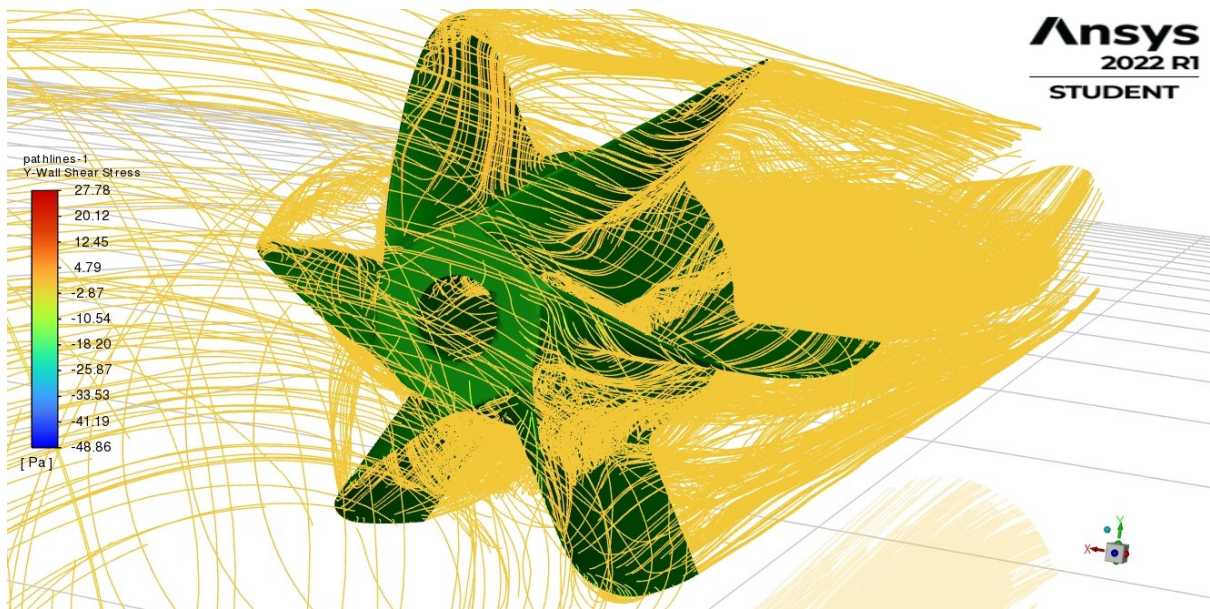


Figure 67 Pathlines of Y-WSS

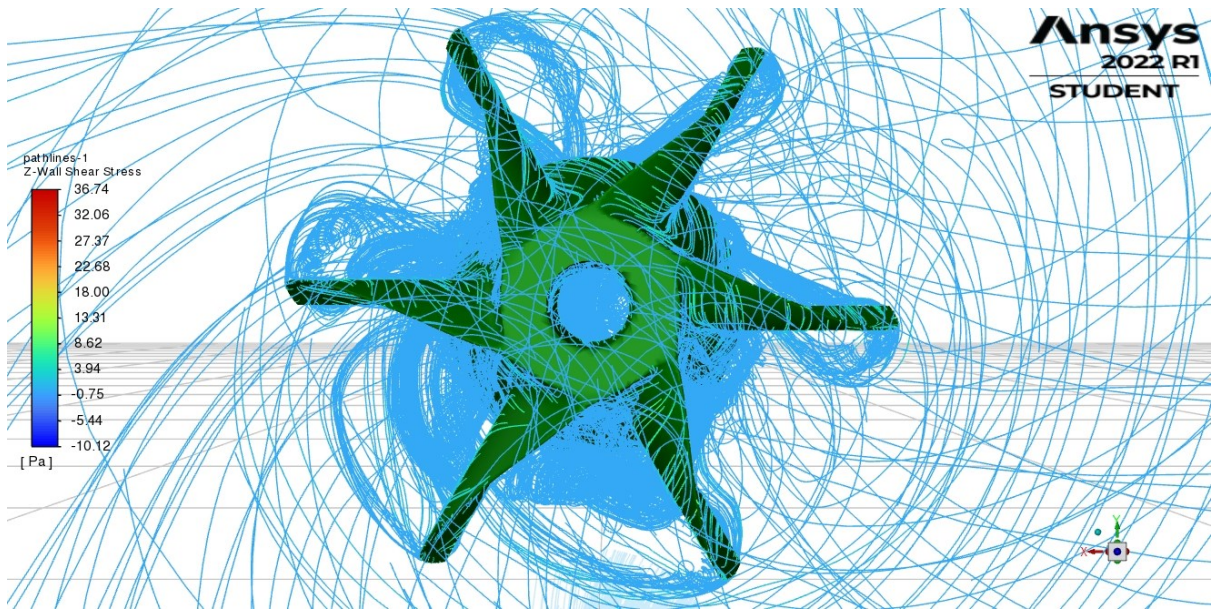


Figure 68 Pathlines of Z - WSS

The values of Y-WSS and Z-WSS are higher than those from first simulation – as it was expected.

Figure 69 shows the contours of Z – WSS on the surface of the impeller.

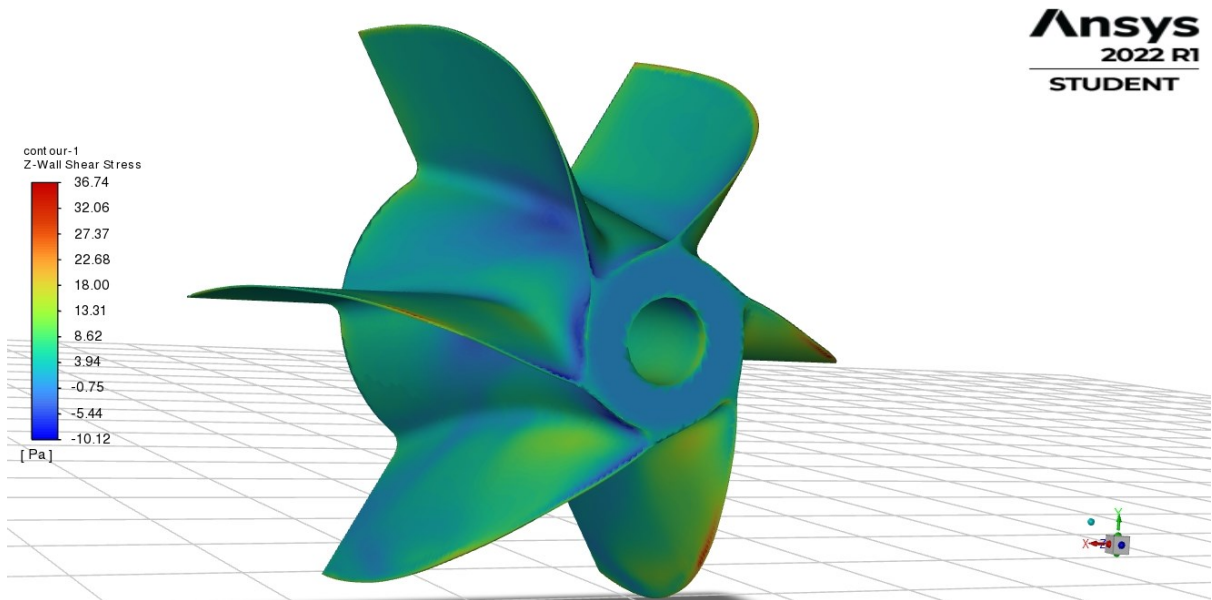


Figure 69 Contours of Z – WSS on the surface of the impeller

Figure 70 shows the profile of Z – WSS through the impeller as the X-Y plot.

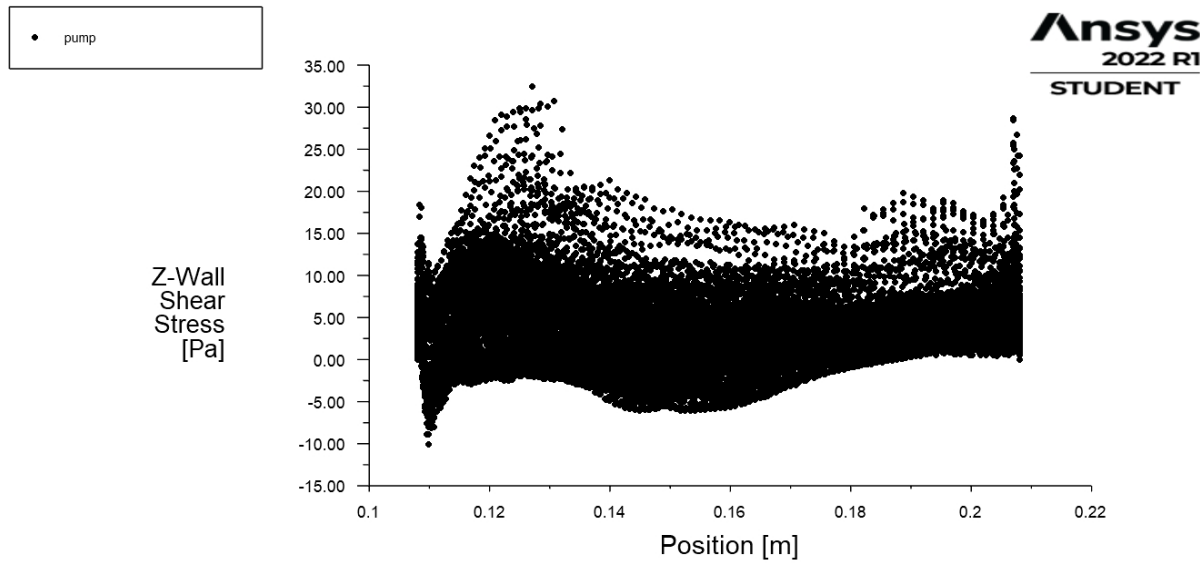


Figure 70 Characteristics of Z – WSS through the impeller

The results are the same as in the first simulation but values are bigger (as expected).

For different visual representation of the WSS, particle tracks simulation were done for YZ plane (as it is shown in figure 71).

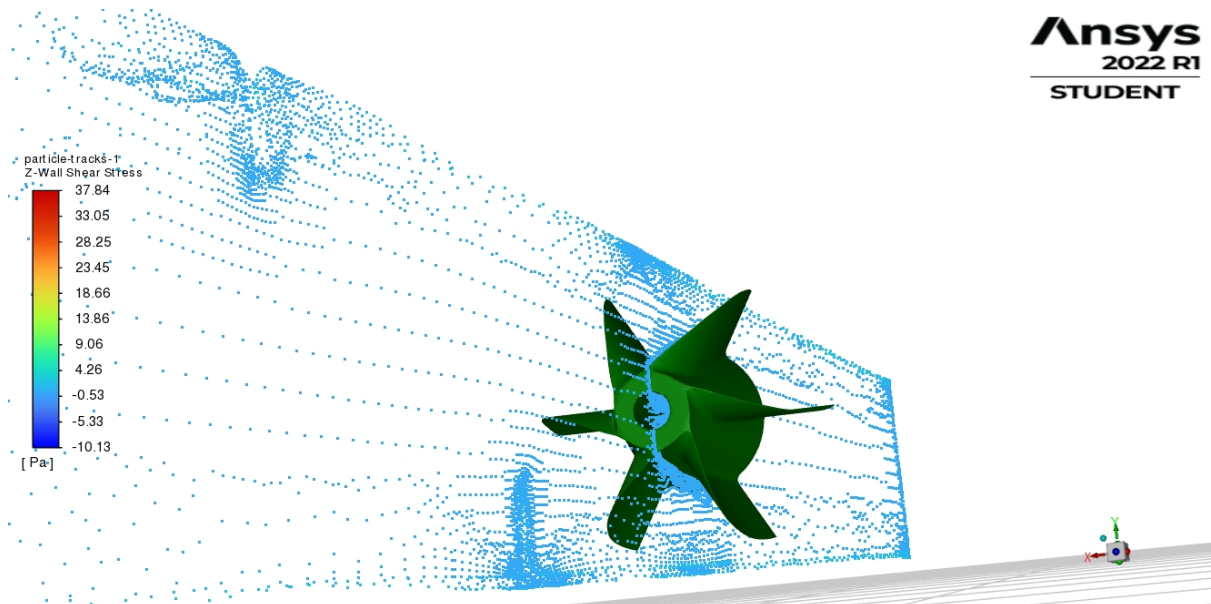


Figure 71 Particle traces on the YZ plane for Z – WSS

Results of Z-WSS and Y-WSS for the YZ plane are as follows:

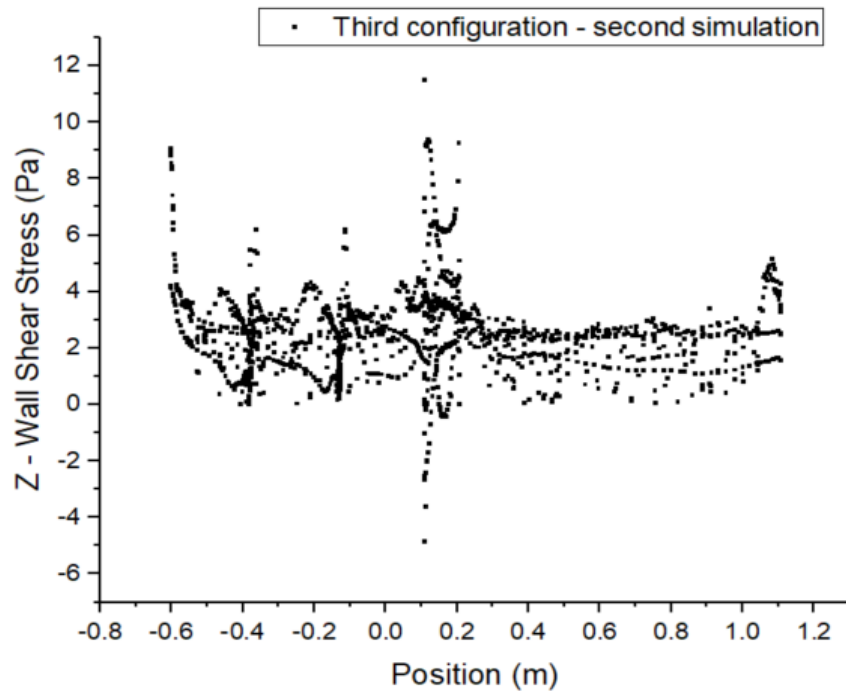


Figure 72 Z- WSS for YZ plane (between blades)

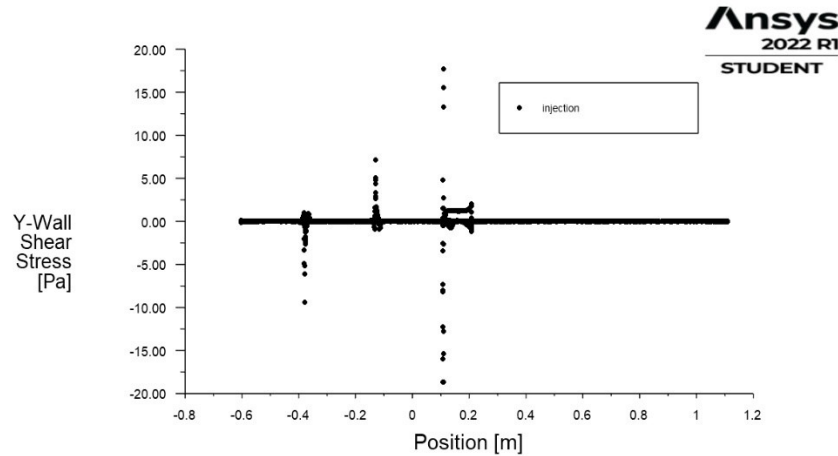


Figure 73 Y – WSS for YZ plane (between blades)

Hydraulic resistance in this case yields:

$$R_H = \frac{\Delta p}{Q} = 2.16 * 10^{12} \frac{kg}{m^4 s}$$

3.3.3 COMPARISON

To summarize, comparison characteristic for Z-WSS through the impeller and for Z-WSS for YZ – plane (between blades) were made to visualize differences between two simulations, and also for validation.

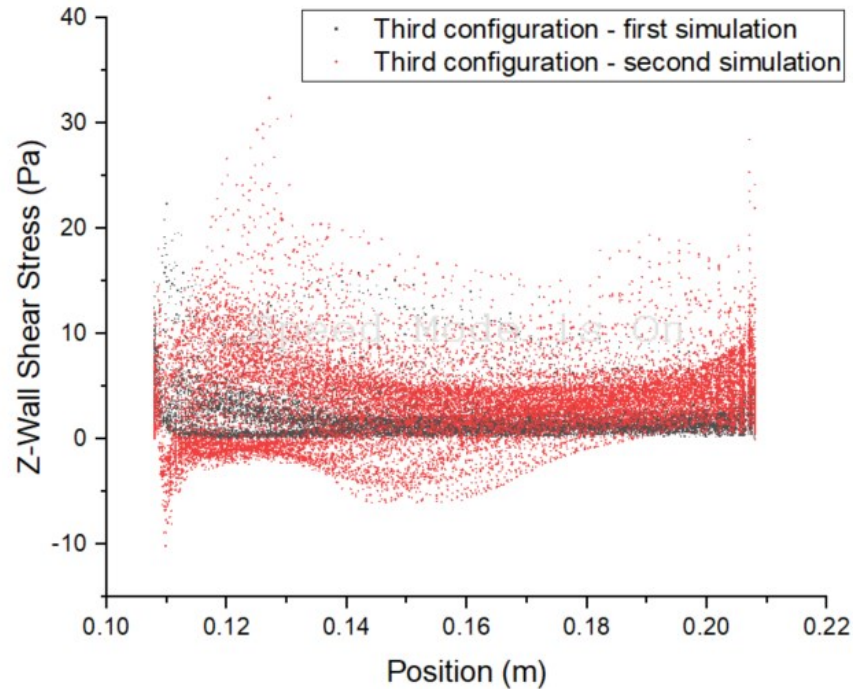


Figure 74 Characteristics of Z-WSS through the impeller for both simulations

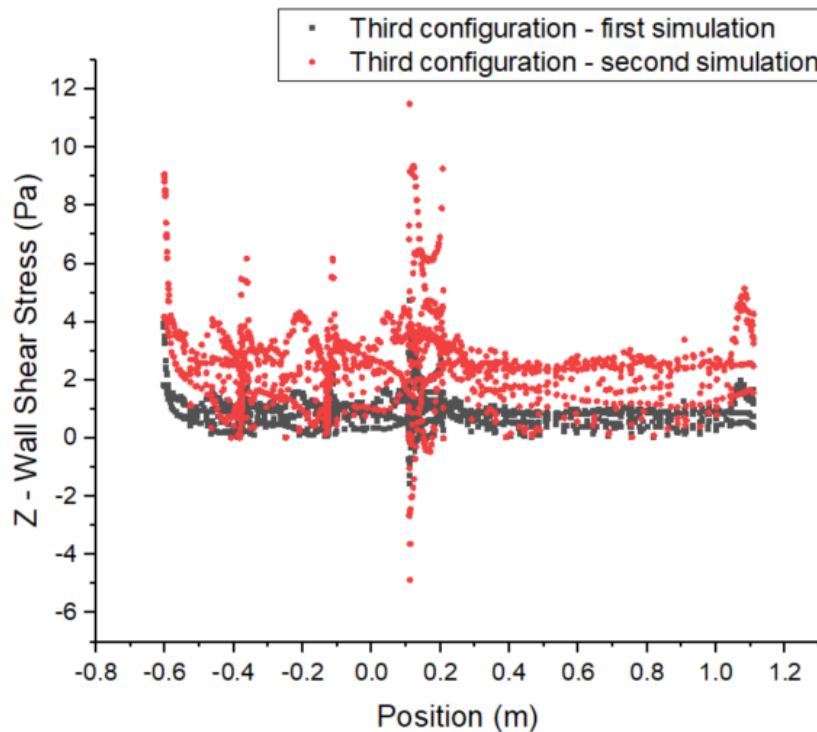


Figure 75 Characteristics of Z-WSS for YZ – plane (between blades) for both simulations.

4. SUMMARY

For total comparison of three configurations, characteristics of Hydraulic resistance were made.

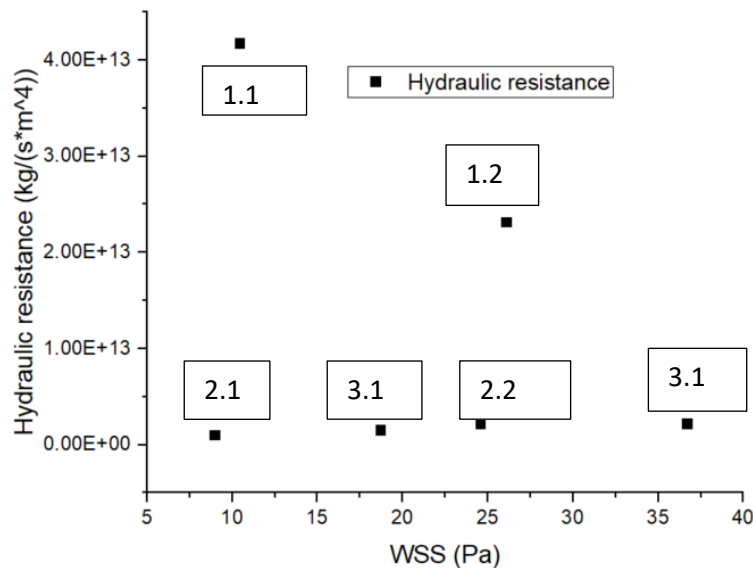


Figure 76 Characteristics of Hydraulic resistance for WSS.

The first number on the graph indicates configuration and the second one indicates simulation; for example 1.2 – first configuration, second simulation.

Taking into consideration the above plot, the most desirable configuration is 2.1 which is impeller with the hole in the centre axis with the inlet velocity = 0.3 m/s.

In terms of the Wall Shear Stress the direction of modifying the geometry of the blades (Leading Edge and Trailing Edge) and elongation of the impeller for elimination of flow separation could be the best solution for optimization.

As far as initial eddy before the impeller is concerned no significant constructive features in terms of optimization for the blood flow through pump was noticed.

REFERENCES

- [1] Blackshear PL, Dorman FD, Steinbach JH. Some mechanical effects that influence hemolysis. *Trans Am Soc Artif Intern Organs* 1965;11:112.
- [2] Kramer C, Sand P, Bleifeld W. Blutströmung und mechanische Hämolyse. *Biomed Tech* 1971;16:164–8